Applied Water Science (2020) 10:49
https://doi.org/10.1007/s13201-019-1138-y

REVIEW ARTICLE

Application of TiO_2 and ZnO nanoparticles immobilized on clay in wastewater treatment: a review

S. Mustapha[1,3] · M. M. Ndamitso[1,3] · A. S. Abdulkareem[2,3] · J. O. Tijani[1,3] · D. T. Shuaib[4] · A. O. Ajala[5] · A. K. Mohammed[6]

Received: 12 August 2019 / Accepted: 27 December 2019 / Published online: 4 January 2020

Abstract

Increase in industrial and anthropogenic activities leads to a decline in water quality. This necessitates the need for the removal of contaminants from industrial and domestic wastewater. Clay minerals are naturally abundant and non-toxic materials that found to be useful for remediation of emerging contaminants from wastewater. This review paper presents an insight into clay, the simplest material (in solgel techniques) for the synthesis of TiO_2 and ZnO, mechanisms of their reactions, analytical techniques used for characterizations, and their nanocomposites for wastewater treatment. Nanomaterials, such as nanoclay, titanium, and zinc oxide, have offered the opportunities of sequestering variety of pollutants in wastewater. TiO_2 and ZnO anchored on clay have been found to be good promising sequesters and have been explored for wastewater remediation via nanotechnology. This water treatment method includes adsorption/absorption, photocatalysis, and microbial disinfection. These nanocomposites provide more active surface sites and reduce the agglomeration of the nanoparticles, but leaching has been their shortcomings. To overcome this, the filtration technique may become significant for the removal and avoidance of fouling of wastewater. This can be achieved through the fabrication of nano-based filters using the nanocomposites.

Keywords Wastewater · Clay · Nanoparticles · Agglomeration · Regeneration

List of symbols

A and B	Redlich–Peterson isotherm constant (L/mg) and exponent, respectively
K_F	Freundlich isotherm constant (mg/g)
Q_m	Maximum monolayer adsorption capacity (mg/g)
n	Adsorption intensity
B_T	Tempkin isotherm constant
ε	Dubinin–Radushkevich isotherm constant
K_s	Sips isotherm model constant (L/mg)
β_s	Sips isotherm model exponent
B and A	Harkin–Jura constants
K_J	Jovanovic isotherm constant (L/mg)
B_K, p and A_K	Koble–Carrigan's isotherm constants
K_e	Elovich equilibrium constant (L/mg)
H, p and F	Jossens isotherm constants
K_{FH}	Flory–Huggins isotherm equilibrium constant (L/g)
θ	Degree of surface coverage
K_1	Hill–de Boer constant (L/mg)
K_2	Energetic constant of the interaction between adsorbed molecules (KJ mol^{-1})
K_i	Kiselev equilibrium constant (L/mg)
C_e	Equilibrium concentration (mg/L)
C_{BET}	Adsorption isotherm relating to the energy of surface interaction (L/mg)

✉ S. Mustapha
saheedmustapha09@gmail.com

1 Department of Chemistry, Federal University of Technology, PMB 65, Bosso Campus, Minna, Nigeria

2 Department of Chemical Engineering, Federal University of Technology, PMB 65, Gidan Kwano Campus, Minna, Niger State, Nigeria

3 Nanotechnology Research Group, Center for Genetic Engineering and Biotechnology, Federal University of Technology, PMB 65, Minna, Niger State, Nigeria

4 Department of Chemistry, Illinois Institute of Technology, 3101 S Dearborn Street, Chicago, IL 60616, USA

5 Department of Industrial Design, Federal University of Technology, Akure, Nigeria

6 Department of Chemistry and Biochemistry, North Carolina Central University, 1801 Fayetteville Street, Durham, NC 27707, USA

C_s	Adsorbate monolayer saturation concentration (mg/L)
q_e	Amount of adsorbate in the adsorbent at equilibrium (mg/g)
q_t	Quantity of adsorbate adsorbed at time t (mg/g)
k_1	Rate constant for the pseudo-first-order sorption (min^{-1})
k_2	Rate constant of the pseudo-second-order kinetic equation (g/mg min^{-1})
$\propto$	Constant related to chemisorption rate
n_{AV}	Avrami model exponent of time related to the mechanism of adsorption
K_{AV}	Avrami constant
t	Time (min)
C_i	Initial concentration of adsorbate (mg/L)
M	Mass of adsorbent (g)
V	Volume of solution (L)
K_{id}	Rate constant for intraparticle diffusion
F	Fraction of adsorbed metal ion at time, t
R	Universal gas constant (8.314 J/mol K)
K_d	Distribution coefficient
T	Temperature (K)
ΔG	Change in Gibbs free energy (kJ/mol)
ΔH	Change in enthalpy (kJ/mol)
ΔS	Change in entropy (J/mol K)

Introduction

Population growth, migration, increasing urbanization, and industrialization over the years have influenced the demand for freshwater resources. It was projected by the World Health Organization (WHO) (2014) that 50% of the global population will be living in water-stressed regions. Industrial production, intensive agriculture, mining, and urban utilization have led to an increase in water use, which eventually have greatly impacted the quality of water available worldwide. Untreated domestic wastewater and industrial effluents contain a variety of organic and inorganic pollutants. Thus the discharge of wastewater from these sources into the ecosystem leads to its pollution.

It has been reported that more than 1.1 billion people globally have access to clean drinking water due to growing populations, and increasing economic activities which have actually led to the deprivation of environmental services (WHO 2015). These factors, coupled with inadequate wastewater management, pose momentous threats to human health and well-being of the human race. Efforts to have access to safe drinking water have been hindered by the release of pollutants to water bodies. These pollutants, which are organic or inorganic in nature, have become an important issue in human development due to their detrimental effects on man and his animals.

Wastewater management approaches for the supply of safe water are difficult due to the stringent and fast-growing demand for clean water. Thus, understanding water treatment methods which are basically aimed at remediating water pollution problems is necessary. In this vein, wastewater treatment methods with high efficacy that will require less processing time and production of non-toxic by-products in the water are urgently required. Several conventional detoxification techniques have been practiced, and these include reverse osmosis, membrane filtration, electrocoagulation, electrodialysis, chemical precipitation, and adsorption, among others. Of all these methods, adsorption is commonly used based on its distinct merits that include energy-saving, cost-effectiveness, simplicity, wide operating range of factors such as pH, concentration, dosage, and temperature. Others include environmental friendliness, fast reclamation of organic and inorganic pollutants, and easy recycling of the sorbent (Sani et al. 2017; Vahidhabanu et al. 2017).

Adsorption can be defined as a surface phenomenon in which pollutants in the form of a molecule known as adsorbate or sorbate are adsorbed on the solid surface called adsorbents or sorbents. This simple method of pollutant removal involves physical or chemical bonding of the contaminants with the functional group's presence in the adsorbents. In recent decades, there have been several natural adsorbents that are used for sequestering of contaminants from wastewater. These include hydrophilic biopolymers such as chitosan (Preethi et al. 2017), carboxymethyl cellulose (Zahedi et al. 2017), and clay minerals (Motshekga et al. 2016). Among these aforementioned polymeric materials, wide documentations on clay minerals for examples kaolinite, bentonite, montmorillonites (smectite), illites, vermiculites, and chlorites that are mainly made up of silica, alumina, water, and weathered rock which could serve as alternative cheap materials for remediation of wastewater, have been studied (Uddin 2016). These minerals are phyllosilicates class of adsorbents with layers that are composed of tetrahedral (T) and octahedral (O) sheets either at 1:1 or 2:1 ratio (Brigatti et al. 2013; Zhu et al. 2016). They possess some unique characteristics among other natural adsorbents, used for adsorption of heavy metals and also serve as a remedy for ailments. Therefore, they can be used as excellent adsorbents for environmental bioremediation and bacteria removal from wastewater (Unuabonaha et al. 2017).

Advanced studies in recent years in nanotechnology have facilitated the application of nanomaterials of high performance in order to tackle problems related to water and wastewater treatment. Nanoscale materials are dimensional substances smaller than 100 nm that exhibit some great physical and chemical features for water treatment (Zhang et al. 2016). These nanoparticles are used as functional

materials in forms of metals/oxides, zeolites, dendrimers, and carbonaceous materials (Bhattachajee et al. 2016).

Recent investigations on nanoparticles have revealed their potentials in wastewater treatment, especially in the area of adsorption. However, there are demerits of the direct use of nanoparticles in wastewater in terms of their aggregation in fluidized systems, difficulty in separation from the treated water and their fates in the treated water (Al-Hamadani et al. 2015; Dale et al. 2015; Lofrano et al. 2016). Hence, the application of nanoparticles due to these disadvantages is very stringent. It is, therefore, imperative that nanoparticles should be encapsulated onto supporting materials such as polymers in order to reduce their release and also increase their reactivity. This approach involves the fabrication nanocomposites of great characteristics that include high surface area, recyclability, and cost-effectiveness. In particular, the high surface area will provide strong interaction between the nanocomposites and pollutants during adsorption.

Nanosize-based adsorbents such as metal oxides, graphene, carbon nanotubes, and nanofibers are widely used for improving treatment of water and wastewater. This is because these nanomaterials are considered to have higher adsorptive performance than conventional adsorbents. The nanosized metal oxides, for example, zinc oxide (ZnO) (Chouchene et al. 2017) and titanium oxide (TiO_2) (Syngouna et al. 2017), have exhibited favorable sorption toward organic and inorganic pollutants. The semiconductor photocatalyst, TiO_2 with external dimension in nanosize, has a wide range of applications in the field of cosmetic materials (Syngouna et al. 2017) and decontamination or mineralization of compounds in water to harmless inorganic anions (Szczepanik et al. 2017). Thus, TiO_2 nanoparticles (T-NPs) have received much attention among researchers due to their extensive characteristics (Nasirian and Mehrvar 2016; Dariania et al. 2016; Lin et al. 2018). It is popularly known that TiO_2 powders in anatase phase have powerful catalytic activities due to their large surface area, surface chemistry, and redox properties. Another inorganic metal oxide, ZnO, serves as a nanoadsorbent due to its non-toxic profile, adsorptive properties, effective antibacterial activity, chemical, mechanical, and thermal stability (Ibrahim and Asal 2017). The use of zinc oxide nanoparticles when compared to titania nanoparticles has higher adsorption rates for heavy metals (Rafiq et al. 2014).

There are challenges in the large-scale utilization of nanoparticles such as TiO_2 and ZnO in water treatment due to difficulty in their separation and recovery after treatment. In addition, the use of both metal oxides nanoparticles for water treatment has some disadvantages, namely: (1) higher colloidal stability in aqueous solution, (2) agglomeration of the nanomaterials at high concentrations, and (3) difficulty in separating and recovering the nanomaterial after use (Martins et al. 2017; Lei et al. 2017). However, steps have been adopted in order to overcome these shortcomings. These include doping and co-doping of metal oxide nanomaterials and immobilization of nanomaterials on suitable matrices (Soltani et al. 2016; Belver et al. 2016). This suitable substrate could function as support in order to overcome the difficulties involved in post-separation and recovery.

Moreover, the support of nanosized semiconductor materials on matrices could help to enhance their activity when compared with ordinary nanomaterials. In this respect, various clay matrices such as kaolinite, montmorillonite, and bentonite have been successfully employed as support. Kaolinite has exceptional crystal chemical features. Therefore, it could act as a suitable matrix for anchoring TiO_2 and ZnO nanoparticles (Dědková et al. 2015; Hadjltaief et al. 2017). Immobilizing and anchoring nanosized TiO_2 and ZnO nanoparticles on the surface of clay minerals provide more active surface sites, reduces the agglomeration of the nanoparticles, and prevents the release of nanoparticles into the environment. Clay nanocomposites have become major components of clay with metallic nanoparticles used in recent research findings in tackling environmental pollutants.

Since, TiO_2 and ZnO nanoparticles are cheap, non-toxic, and capable of removing emerging contaminants, and given the fact that rural communities are affected by contaminants from wastewater, cheaper and environmentally friendly methods for the wastewater treatment need to be adopted for water and wastewater treatment. Thus, this review of literature examines the simple methods for the preparation of TiO_2 and ZnO and discusses some classes of clay and their adsorptive and photocatalytic characteristics for their possible employment in the removal of contaminants from wastewater.

Wastewater treatment

Different methods have been developed and used for the treatment of wastewater. Some of the adopted techniques are centrifugation (Peeters 2015), filtration (Cardenas et al. 2016), flotation (de Oliveira da Mota et al. 2015), evaporation (Li et al. 2016), distillation (Ji 2018), ion exchange (Tan et al. 2017), precipitation (Sun et al. 2017), electrolysis (Huang et al. 2016), electrodialysis (Akhter et al. 2018), adsorption (Guillaume et al. 2018; You et al. 2019), crystallization (Lu et al. 2017), micro and ultra-filtration (Pinto et al. 2017), sedimentation and gravity separation, reverse osmosis (Venzke et al. 2017), and coagulation (Mousa and Hadi 2016). However, these prevailing technologies have some setbacks such as being time-consuming and costly and leading to the generation of toxic sludge. Therefore, there is an urgent need to overcome these shortcomings. Among these methods, adsorption is found to be the most promising owing to its simplicity, environmental friendliness,

adsorption efficiency, and cost-effectiveness. Adsorption technology depends on the utilization of either modified or unmodified adsorbents controlled by parameters such as contact or residence time, pH, concentration, temperature, and adsorbent dosage (Al-Essa and Khalili 2018). The phenomenon governing the uptake of pollutants from wastewater onto different adsorbents is strong forces and weak bondings. Adsorption is established by batch and column adsorption studies. The batch adsorption is widely utilized for wastewater treatment based on its simplicity and general application on a small scale for the assessment of adsorptive capacities of adsorbents in static conditions.

Generally, some theoretical approaches have been employed for the explanation of the interactions between sorbents/adsorbents and sorbates/adsorbates, and these include equilibrium isotherm, kinetic, and thermodynamic studies. Adsorption equilibrium, on the one hand, explains the physicochemical processes involved in sorption and kinetic measures. The degree of the transport mechanism of wastewater in adsorbent which comprises of the external mass transfer of the sorbate from the bulk solution to the surface of the sorbent, the internal diffusion of the sorbate to the adsorption site, and the overall adsorption process (González and Pliego-Cuervo 2014), while thermodynamic describes the attractive and repulsive interaction such as electrostatic or dipole and van der Waals, expressed in terms of free energy. The thermodynamic parameters at different temperature are computed using the following equations (You et al. 2018):

$$K_{\mathrm{d}} = \frac{q_{\mathrm{e}}}{C_{\mathrm{e}}} \tag{1}$$

$$\Delta G = -RT \ln K_{\mathrm{d}} \tag{2}$$

$$\Delta G = \Delta H - T\Delta S \tag{3}$$

Over the years, various equilibrium isotherms and kinetic models have been established by researchers in order to explain the dynamic adsorption behavior of pollutants onto adsorbents. Table 1 shows some equilibrium isotherms and kinetic models proposed for the adsorption of pollutants in wastewater samples.

Nanotechnology for water sustainability

The applications of physical, chemical, and biological processes to wastewater treatment have some disadvantages due to the presence of some non-biodegradable pollutants which frequently are toxic to microorganisms, man, and his farm animals. Hence, wastewater treatment technology with prolific efficiency and low cost is always required for wastewater treatment. As a result of this, nanotechnology, in lieu of other treatment methods, has shown some potential for wastewater remediation by adsorption (Zekic et al. 2018). Thus, in recent years, researchers have shown vast interests in this topic as an improvement over existing methods.

Nanotechnology is a field of nanoscience where nanomaterials with dimensions less than 100 nm are developed in various forms and used for many purposes (Jeevanandam et al. 2018). These include nanotubes, nanowires, particles, films, fiber, colloids, nanorods, and quantum dots or nanocrystals as shown in Fig. 1.

The environmental applications of nanotechnology include the removal or degradation of hazardous materials, sensors for the level of environmental pollution, and pollution preventer (Khan et al. 2017). The unique properties of these nanomaterials are high reactivity, large surface area, easy separation, small size, high catalytic properties, and presence of many active sites for binding of pollutants.

In general, these nanomaterials are categorized into: (1) nanoadsorbents (2) nanomembrane (3) nanocatalysts, and (4) nanofiber. Numerous works have been done using nanoadsorbent, nanofiber, and nanocatalyst materials in water nanoadsorption technology in recent years (Rafati et al. 2019; Voigt et al. 2019; Mousavi et al. 2019). The properties of these nanomaterials are responsible for their high adsorption capacities in wastewater treatment. The commonly used materials for wastewater remediation are clay, activated carbon and silica, metal oxides such as titanium oxide, zinc oxide, nickel oxide, iron oxide, tungsten oxide, copper oxide, and alumina. Along with other metal oxides nanomaterials, TiO_2 and ZnO have attracted the interest of scientists in wastewater treatment processes. Therefore, nanomaterials have effectively contributed to the establishment of robust and cost-effective water adsorption techniques (Gehrke et al. 2015).

Synthesis and characterization of nanoparticles

Several techniques have been employed for the synthesis of titanium oxide and zinc oxide nanoparticles. These have been categorized into three major classes: (1) liquid phase, (2) gas phase, and (3) vapor phase.

The wide employment of these materials for nanomaterial production is, as a result, their properties such as environmental friendliness and moderate prices. Among the techniques used for the production of these nanomaterials, wet chemical methods have been known to be the best, and these include microemulsion, hydrothermal/solvothermal, precipitation, and solgel methods which have been well studied. Of these, the solgel method is reported to be the simplest and the most economical thus the most often used to

Table 1 List of adsorption isotherms and kinetics models used for the elucidation of pollutants removal from wastewater

Model	Equation	Linear form	References
Isotherm	Freundlich	$\ln q_e = \ln K_F + \frac{1}{n} \ln C_e$	Freundlich (1906)
	Langmuir	$\frac{C_e}{q_e} = \frac{1}{bQ_m} + \frac{C_e}{Q_m}$	Langmuir (1916)
	Tempkin	$q_e = a + B_T \ln C_e$	Temkin and Pyzhev (1940)
	Dubinin–Radushkevich	$\ln q_e = \ln Q_m - k\varepsilon^2$	Dubinin and Radushkevich (1947)
	Redlich–Peterson	$\ln \frac{C_e}{q_e} = \beta \ln C_e - \ln A$	Redlich and Peterson (1959)
	Sips	$\beta_s \ln (C_e) = -\ln \left(\frac{K_s}{q_e}\right) + \ln (a_s)$	Sips (1948)
	Harkin–Jura	$\frac{1}{q_e^2} = \frac{B}{A} - \left(\frac{1}{A}\right) \ln C_e$	Livingston (1949)
	Jovanovic	$\ln q_e = \ln q_{max} - K_J C_e$	Jovanovic (1969)
	Koble–Carrigan	$\frac{1}{q_e} = \left(\frac{1}{A_K C_e^p}\right) + \frac{B_K}{A_K}$	Koble and Corrigan (1952)
	Jossens	$\ln \left(\frac{C_e}{q_e}\right) = -\ln (H) + F q_e^p$	Jossens et al. (1978)
	Elovich	$\ln \left(\frac{q_e}{C_e}\right) = \ln K_e q_m - \frac{q_e}{q_m}$	Elovich and Larinov (1962)
	Flory–Huggins	$\ln \left(\frac{\theta}{C_o}\right) = \ln K_{FH} + n_H \ln (1-\theta)$	Flory (1941)
	Hill–Deboer	$\ln \left[\frac{C_e(1-\theta)}{\theta}\right] - \frac{\theta}{1-\theta} = -\ln K_1 - \frac{K_2 \theta}{RT}$	De Boer (1953)
	Kiselev	$\frac{1}{C_e(1-\theta} = \frac{K_i}{\theta} + K_i K_n$	Kiseler (1958)
	Brunauer–Emmett–Teller	$\frac{C_e}{q_e(C_s - C_e)} = \frac{1}{q_m C_{BET}} + \frac{(C_{BET}-1)C_e}{q_m C_{BET} C_s}$	Bruanuer et al. (1938)
Kinetic	Pseudo-first-order	$\ln (q_e - q_t) = \ln q_e - k_1 t$	Lagergren (1898)
	Pseudo-second-order	$\frac{t}{q_t} = \frac{1}{q_e^2 k_2} + \frac{t}{q_e}$	
	Elovich	$q_t = \propto \ln (a\alpha) + \alpha \ln t$	Roginsky and Zeldovich (1934)
	Avrami	$\ln [-\ln (1- \propto)] = n_{AV} K_{AV} + n_{AV} \ln t$	Avrami (1940)
	Boyd	$F = \frac{q_t}{q_e} = 1 - \frac{6}{\pi^2} \exp (-B_t)$	Boyd et al. (1947)
	Bangham	$\log \left[\log \left(\frac{C_i}{C_i - q_t M}\right)\right] = \log \left(\frac{K_j M}{2.303V}\right) + \alpha \ln t$	
	Weber and Morris	$q_t = K_{id} \sqrt{t} + A$	Weber and Morris (1963)
	Fractional power	$\log q_t = \log K + V \log t$	

synthesize TiO_2 (Dodoo-Arhin et al. 2018) and ZnO (Kaneva et al. 2016) nanoparticles. However, there are still ongoing researches on the synthesis of TiO_2 and ZnO nanoparticles using the solgel method.

Solgel method

Among the wet chemical methods, the solgel is a sophisticated method also known as chemical solution deposition which is the most often used method for the production of TiO_2 and ZnO and practically used in the field of material science, wastewater treatment, and ceramic engineering. In general, the solgel method mainly encompasses the use of chemical solutions which act as the precursors for the gel of either separate or network particles. The method helps to control the stability and phase formation of the precursors. During this process, the gel which contains alcohol, precursor, and water constitutes the interconnected porous matrix. Therefore, an integrated network gel-like diphasic solution containing both liquid and solid phases is produced, while the typical precursors of the metal oxide nanoparticles on the addition of water form a colloid (Kumar et al. 2015). At this stage, the particle density may be low in such a way that some amount of fluid may need to be evacuated for a complete gel-like property to be established. This can be achieved firstly, by allowing sedimentation to occur and then the liquid is poured off, and secondly, by centrifugation for phase separation.

The removal of the remaining solvent phase needs a drying process to enable densification and reduction in size. Afterward, the metal oxide as an aerogel would be obtained either by evaporation of the solvent used during the time

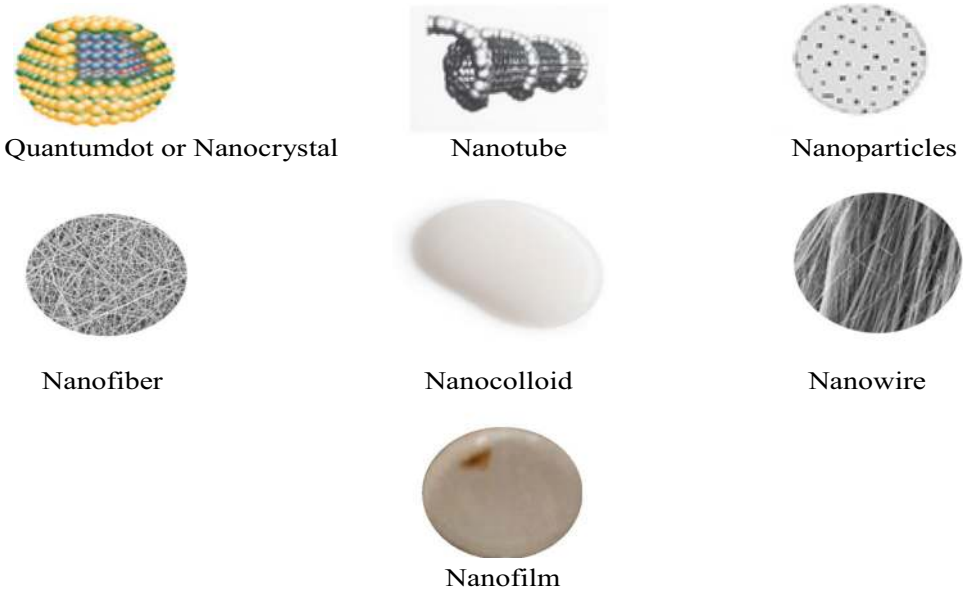

Fig. 1 Images of some nanomaterials

of washing from the wet gel or by supercritical drying as shown in Fig. 2.

Importantly, the produced gel can be classified into two forms depending on the kind of solvent utilized, namely aqueous (use of water) and non-aqueous (use of organic

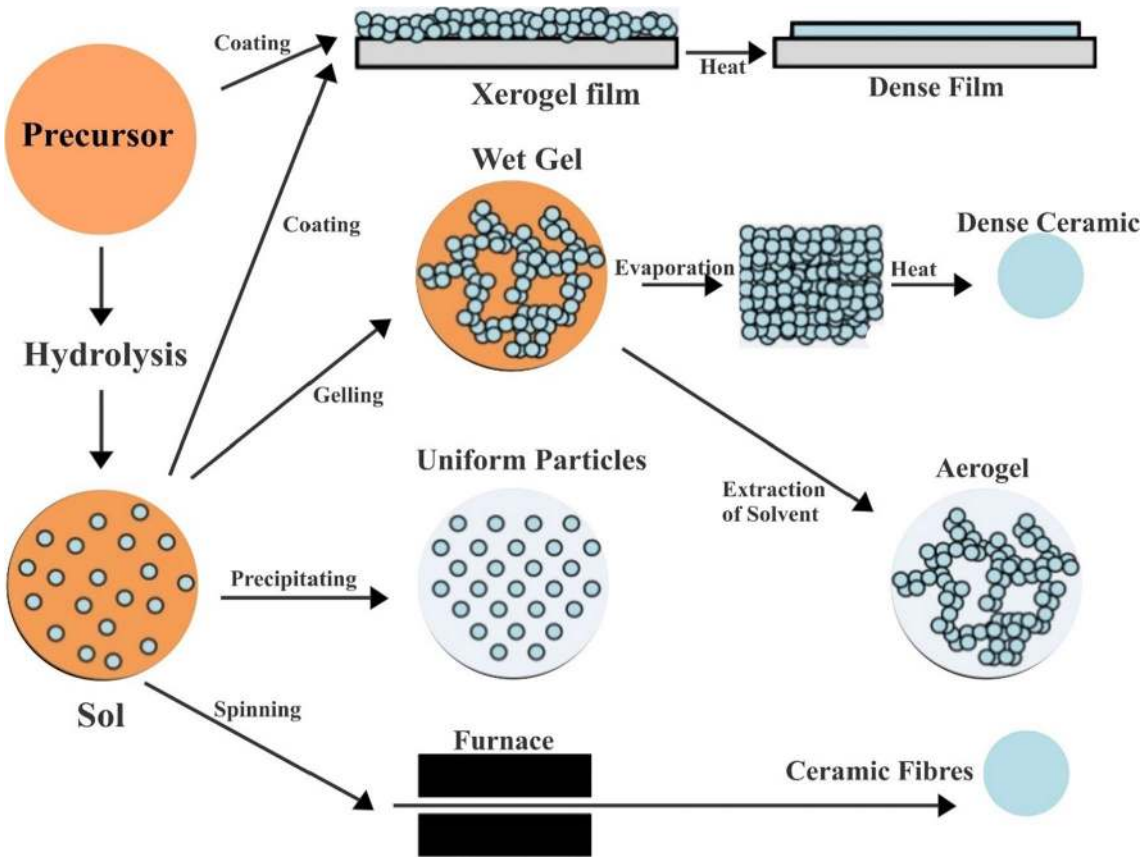

Fig. 2 Different stages and routes of the solgel method

solvent) solgel (Rao et al. 2017). Further treatment of the wet gel could also convert the gel into dense glass or ceramic, which offers high purity, uniform nanoparticles at low-temperature processing, molecular homogeneity, and fine particle size. However, parameters such as the addition of reactants, temperature or calcination, pH, and solubility of chemicals in the solvents affect the molecular homogeneity of the gel (Bahar et al. 2017).

Synthesis and mechanism of TiO_2

TiO_2 is a white solid crystalline powder insoluble in water. It has been considered a non-toxic material that can be used for the production of nanomaterials with a high concentration of hydroxyl groups, stability, and catalytic efficiency (Bagheri et al. 2014). TiO_2 is also known as titania, which naturally exists in three forms, namely, anatase, rutile, and brookite. Both the anatase and rutile forms have tetragonal shapes, while brookite has orthorhombic shape. Other phases that can be synthesized are TiO_2B, TiO_2H (hollandite-like form), TiO_2R (ramsdellite-like form), TiO_2II (α-PbO_2-like form), akaogiite (baddeleyite-like form, 7 coordinated Ti), TiO_2O, cubic form, and TiO_2 OII (cotunnite $PbCl_2$ like) (Ullatti and Periyat 2017). To synthesize anatase, rutile and brookite TiO_2 nanoparticles, hydrolysis, condensation, and calcination are employed (Fig. 3).

The solgel method is commonly used to synthesize TiO_2 nanoparticles, and the most commonly used precursors are titanium(IV) tetraisopropoxide (TTIP), titanium chloride, titanium(IV) tert-butoxide, bis (cyslooctatraene) titanium, tetraisopropylorthotitanate (TIPT), potassium titanium oxalate (KTO), butyl titanate (TBT), and titanium(IV) butoxide (Morales et al. 2013; Singh et al. 2017). During this process, the formation of colloid is as a result of hydrolysis and polycondensation reactions. An acid and a base help in the hydrolysis of the precursor. However, the four stages that occur during the solgel formation are hydrolysis, condensation, growth, and agglomeration of particles. Thus, this process proceeds by hydrolytic polycondensation of titanium precursors being alkoxides or chlorides in the presence of solvents, modifiers, and organic templates. The reaction starts with hydrolysis, which is the formation of Ti–OH moieties by the substitution reaction of water with Ti–OR groups. The precursors undergo condensation reactions to produce Ti–O–Ti by oxolation or Ti–OH–Ti bonds by olation (Islam et al. 2017). The mechanisms for the formation of TiO_2 nanoparticles are presented in Fig. 4.

Various researchers have outlined some steps for the synthesis of TiO_2; for instance, about 20 cm^3 of titanium tetraisopropoxide solution was added to isopropanol solution in a beaker, and the resultant mixture stirred at 80 °C for 1 h. To the mixture, 8 cm^3 of concentrated nitric was added and kept under constant stirring at 60 °C for 6 h after which a gelatinous solgel solution was obtained. The obtained solgel was calcined at the 300 °C for 2 h to obtain TiO_2 nanocrystals by Sharma et al. (2014).

According to Devi et al. (2014), titanium tetraisopropoxide was used as a precursor and then mixed with ethanol, deionized water and adjusted to the pH of 1.5 with HCl. This was stirred for 30 min, and further 10 cm^3 of deionized water was added and then stirred for 2 h. The resultant mixture was dried at 120 °C for 1 h.

A little modification was made by Phonkhokkong et al. (2016) for the preparation of the nanoparticles. About 9 cm^3 of titanium (IV) butoxide ($Ti(OBu)_4$) solution was measured into 35 cm^3 of ethanol and then stirred for 2 h.

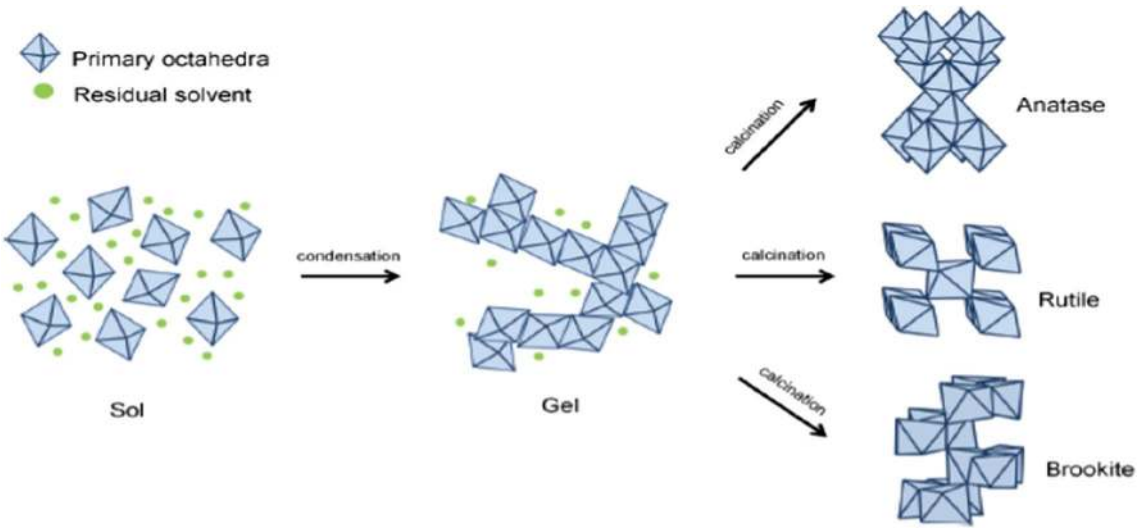

Fig. 3 Steps for the synthesis of crystalline anatase, rutile, and brookite TiO_2 nanoparticles (Yahaya et al. 2017)

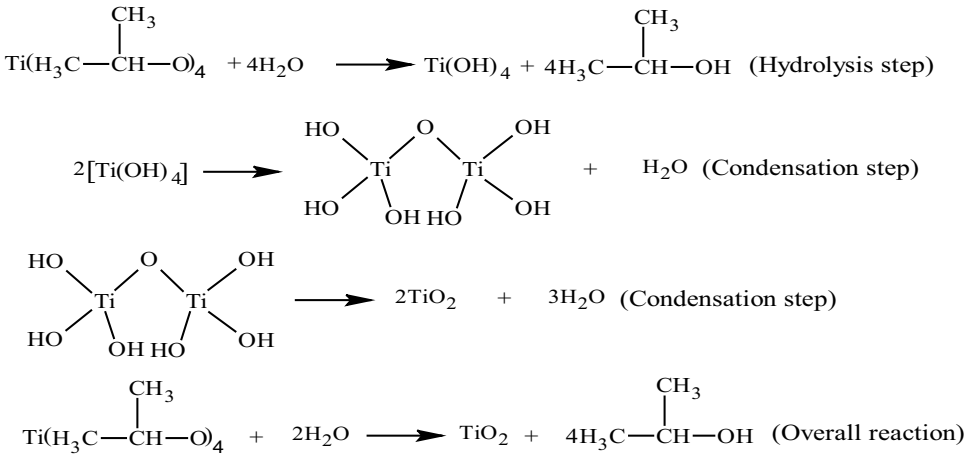

Fig. 4 Hydrolysis and condensation reactions of titanium isopropoxide for TiO_2 production

A hydrolyzed solution was obtained and further stirring was done for 2 h. Comprehensive washing was done on the white precipitate obtained with ethanol and water and then dried at 100 °C for 3 h. This was then calcined at 400 °C for 2 h.

Titanium isopropoxide ($Ti(OCH(CH_3)_2)_4$) and citric acid ($((C_3H_5O(COO)_3)H_3{\cdot}H_2O$) were used as precursors at a mole ratio of 1:3, respectively, according to the method adopted by Pookmanee and Phanichphant (2014). The solutions were adjusted with ammonium hydroxide (NH_4OH) to the pH of 2, 4, and 6. The final solutions were firstly oven-dried at 80 °C for 24 h and calcined at 400 and 800 °C, respectively, for 2 h.

According to Liu et al. (2014), dibutyl phthalate was used as a precursor, and a certain amount of it was measured into a beaker that contained 20 cm^3 of ethyl alcohol. The solution was stirred for 60 min, and then drops of concentrated HCl were added to the mixture. The authors failed to ascertain the exact pH of the solution. The gel was oven-dried at 80 °C for 7 h and calcined at 550 °C for 2 h.

The synthesis of TiO_2 was performed by Yin et al. (2016) using 10 cm^3 of tetrabutyl titanate to which 15 cm^3 of deionized water, 8 cm^3 of 5% nitric acid, and 300 cm^3 ethanol were added. In their study, polyacrylamide (PAM) and polyethylene glycol (PEG) were used as composite templates to produce mesoporous TiO_2 samples with large specific surface area and high crystallinity. Vigorous stirring was done on the resulting mixture to produce a white gel, dried at 80 °C for 1 h, and then two-step calcined at 500–700 °C and 500 °C, respectively.

TiO_2 colloidal solution was prepared by hydrolysis of titanium tetraisopropoxide (TTIP) by Kavitha et al. (2014) who reacted 1 cm^3 of titanium tetraisopropoxide with 4 cm^3 of acetic acid. The resultant mixture was hydrolyzed with 10 cm^3 of distilled water and vigorously stirred for 1 h. This was kept in an oven at 100 °C and then annealed at 300 and 600 °C for 1 h.

Bahar et al. (2017) synthesized TiO_2 nanoparticles using $TiCl_4$ as the precursor. $TiCl_4$ was added to ethanol, isopropanol, and butanol at a molar ratio of $TiCl_4$/alcohol of 1:10. The solutions were stirred and calcination process was performed at 450 °C. Effects of alcohol type, calcination, gelatinizing time, and microwave exposure on the particle size, morphology, crystallinity and particle-phase were studied.

Divya et al. (2017) prepared double precursors for the synthesis of TiO_2 nanoparticles. The first precursor was made by adding TTIP with 2-propanol. To this solution, 200 cm^3 of distilled water was added and 2 M nitric acid was used to adjust the pH to 2. A 5 cm^3 of TTIP taken to be the second precursor was added in drops to the firstly prepared solution and allowed to settle down under a temperature of 60 °C for 30 min. The sol was washed with distilled water and methanol to remove the impurities. The resultant precipitate was dried to obtain a fine white powder of TiO_2. In another study, about 50 cm^3 of deionized water was added to 3.5 cm^3 of the $TiCl_4$. To this mixture, a drop of ammonium hydroxide (NH_4OH) was added to obtain a yellow gel. The formation of the yellow color was taken as an indication of the presence of $Ti(OH)_4$. The solution was stirred for 30 min and then centrifuged. The precipitate was allowed to dry at 200 °C for 4 h. The amorphous white TiO_2 was calcined in the furnace at 250, 400, and 600 °C for 4 h (Hayle and Gonfa 2014). Moussaoui et al. (2017) prepared nanocrystalline powders of TiO_2 xerogel and aerogel using an acid-catalyzed solgel method. The synthesis of these nanoparticles began by reacting the solution of TTIP in isopropyl alcohol with water. The solution was stirred at room temperature and the formation of white precipitate known as $Ti(OH)_4$ was left overnight in order to ensure complete hydrolysis. The alcohol was then separated from the mixture using rotary evaporator, and drops of acetic acid were added. The precipitate was transferred to a Teflon-lined stainless-steel autoclave and heated at 300 °C at 100 bars for 1 h to

produce TiO_2 aerogel. However, the second class of the nanoparticles known as TiO_2 xerogel was prepared by drying at 200 °C under an atmospheric condition for 10 days.

Table 2 describes the characterization, experimental conditions, and crystallite sizes of synthesized TiO_2 nanoparticles using solgel.

Table 2 Summary of synthesized TiO_2 nanoparticles via solgel method from 2013 to 2018

Crystallite size (nm)	Characterization	Raw material	Condition	References
–	XRD, FTIR, SEM, TEM, TGA	Titanium isopropoxide, tetra-*n*-butyl orthotitanate, ammonia, sodium hydroxide, nitric acid	pH 10	Gómez-de-Salazar et al. (2016)
8	XRD, DRS	Titanium isopropoxide, pluronic P123, acetylacetone, nitric acid	Calcined at 400 °C	Smirnova et al. (2017)
9–23	XRD, SEM, EDX	Tetra-*n*-butyl orthotitanate, hydrochloric acid, ammonia solution, methanol	pH 4–6, calcination temperature of 450–750 °C	Dalvandi and Ghasemi (2013)
13	XRD, HRTEM-EDXS, XPS, RAMAN, UV–Vis	Titanium butoxide, ethanol, hydrochloric acid	Calcined at 400 °C	Mathews et al. (2014)
9–12	TGA, XRD, TEM, FTIR, UV–Vis	Titanium isopropoxide, glacial acetic acid, gelatin	Calcination temperature of 500 °C	Bagheri et al. (2014)
8.27–19–96	XRD, BET, XPS, UV–Vis, RAMAN, FESEM, FTIR, HRSEM	Titanium isopropoxide, ethanol, nitric acid, ammonia solution	Aging time for 24 h, calcination temperature of 400–600 °C	Kassahun et al. (2017)
10	XRD, EDS, TEM, FTIR, UV-DRS, UV–Vis	Titanium oxysulfate, ammonia	Calcined at 400 °C	Khade et al. (2016)
–	XRD, FESEM, FTIR, DRS, EDX, PL	Titanium isopropoxide, acetic acid	Calcination temperature of 400 °C	Marami et al. (2018)
~6	XRD, SEM, FTIR	Titanium isopropoxide, distilled water, nitric acid	Calcined at 400 °C	Thangavelu et al. (2013)
58–111	XRD, AFM, FETEM, PL	Titanium chloride, ethanol	Gelatinization time, calcination temperature of 500–900 °C	Sabry et al. (2016)
–	XRD, SEM, TEM, BET	Titanium isopropoxide, nitric acid, ethanol	–	Sheikhnejad-Bishe et al. (2014)
8–10	XRD, TEM, DRS-UV	Titanium isopropoxide, acetic acid, sodium hydroxide	pH 2–5, aging time of 0–21 days	Fajriati et al. (2017)
10	XRD, UV–Vis, FTIR, FESEM, EDS	Titanium isopropoxide, ethanol, distilled water	Calcination temperature of 450 °C	Sakthivel and Jagannathan (2017)
17	XRD, UV-DRS, BET, FESEM, HRSEM, EDXA	Titanium isopropoxide, deionized water	Calcined at 450 °C	Govindaraj et al. (2015)
–	XRD	Titanium isopropoxide, distilled water	Calcination at 400 °C	Oganisian et al. (2015)
15 and 32	XRD, TEM, SEM, FTIR	Titanium tetrachloride, ethanol	pH 1–2, calcined at 500 °C and 900 °C	Haider et al. (2015)
10	XRD, SEM, FTIR, UV–Vis	Titanium isopropoxide, ethanol, water nitric acid	Oven-dried at 50 °C	Kaler et al. (2016)
–	XRD, SEM, EDX	Titanium tetrachloride, distilled water, ammonia hydroxide	pH 1.1–10, annealed at 500–800 °C	Elbushra et al. (2018)
7.64–11.21	XRD, TEM, BET, DR-UV–Vis, TG-DSC	Tetrabuylt titanate, nitric acid, ethanol, polyethylene glycol, polyacrylamide	Calcination temperature of 500–700 °C	Yin et al. (2016)
29.8	XRD, TEM, SEM, FTIR	Titanium isopropoxide, 2-propanol, distilled water, hydrochloric acid	Calcined at 500 °C	Nachit et al. (2016)
19.11	UV, XRD, SEM, FTIR	Titanium isopropoxide, ethanol, distilled water	Calcined at 400 °C	Mallika and Narsaiah (2017)

In general, the solgel method which consists of the transformation of a system from a liquid phase (sol) to a solid phase (gel) as discussed above, involves the use of various precursors such as organic alkoxides and acetates, in addition to inorganic salts like chlorides. Alcohols are greatly used among various kinds of solvents, although some other solvents could be used for some alkoxides.

Using this method, some parameters such as the order of addition of reactants, the temperature, stirring time, the ratio of water to titanium, the solubility of reagents in the solvent, and the pH affect the homogeneity of the gel. Calcination temperature and pH are paramount factors which help in giving the nanoparticles better surface areas. Among the researchers who worked on the production of TiO_2-NPs using the solgel method and examined some of the properties of the produced nanoparticles using various instruments such X-ray diffraction (XRD), scanning emission microscope (SEM), photoluminescence (PL), high-resolution transmission microscopy (HRTEM), Brunauer–Emmett–Teller (BET), thermogravimetric analysis (TGA), and selected area electron diffraction (SAED) were Sharma et al. (2014), Phonkhokkong et al. (2016), and Kavitha et al. (2014).

Factors affecting TiO_2 nanoparticles

The forms of TiO_2 depend on the arrangement of titanium and oxygen atoms in the crystal lattice. Therefore, it has been reported that the solvent, precursor type, particle size, calcination temperature, pH, additives, and stirring time affect solgel-synthesized TiO_2 nanoparticle phases (Agarthan et al. 2013; Islam and Basu 2015). It has been reported that the particle sizes of the synthesized nanoparticles increase as their surface areas increase (Chen et al. 2014b; Pavel and Radovan 2015). Thus, this section offers a brief discussion on the influence of some parameters on the formation of TiO_2 nanoparticles.

Effect of calcination

Calcination is a thermal treatment process in the absence of a limited supply of air required for thermal decomposition. The effect of calcination temperature on the phase of TiO_2 from 100 to 1000 °C was evaluated by Pavel and Radovan (2015). The authors reported that at 500 °C, the observed peaks conformed to the anatase phase, but as the peak grew to 800 °C, the anatase phase was transformed to rutile. They concluded that 600 °C was convenient to achieve higher efficiency nanoparticles due to the finer grains of the anatase phase of TiO_2 synthesized.

Abdullah et al. (2017a, b) demonstrated the effect of calcination temperature on nanocomposite used in the photocatalytic degradation of phenol under the visible light. The nanocomposite (ZnO/TiO_2) produced at 600 °C was found to be more effective in the destruction of the pollutant as a result of the formation of hydroxyl radical on the surface of the nanocomposite. They also deduced that the formation of anatase phase enhanced the degradation of the targeted pollutant.

Thus, calcination temperature controls the crystalline phase of TiO_2 nanoparticle, their homogeneity, and surface area. Also, the particle size of TiO_2 was found to increase with calcination temperature, suggesting that different calcination temperatures affect the degradation of pollutant in wastewater.

Furthermore, calcination temperature affects the application or activity of a particular nanoparticle produced. In this vein, He et al. (2014) indicated that uncalcined TiO_2 showed a low photocatalytic effect as a result of low crystallization. With an increase in calcination temperature, the photocatalytic effect of the TiO_2 increased due to the high crystallization of the particles and evacuation of CO_2 from the system. In another research conducted by Wang et al. (2017) on TiO_2 nanoparticles at temperature range of 300–600 °C for photodegradation of an organic pollutant, it was observed that at lower temperatures, the crystals of TiO_2 were not formed, but as the calcinating temperature increased, crystallization and change of phase were observed. During the degradation of the organic pollutant, the removal efficiency became low signifying the importance of TiO_2 phase in its application. A recent contribution made by Haq et al. (2018) submitted that decrease in the surface area and pore volume was observed as the temperature of calcination increased and opined that these were as a result of rearrangement and growth of TiO_2 crystallites.

Effect of pH

The pH of a medium significantly affects crystal structure and surface morphology such as the size and entanglement of TiO_2 nanostructures (Xue et al. 2014; Selman et al. 2014; Mohite et al. 2015). Due to the small particle size of nanoparticles, the van der Waals interaction is significant, and this increases exponentially as the particle size decreases, thus favoring the growth of clusters. Ibrahim and Sreekantan (2010) reported that lower acidity promotes anatase structure while high acidity results in rutile phase formation. This shows that the degree of crystallinity of anatase is pH-dependent and lower acidity enhances the crystallinity, which also promotes the formation of big crystallite size. Tsega and Dejene (2017) reported that the morphology and crystallinity of TiO_2 nanoparticles depend on the pH of the precursor solution. Lower acidity promotes anatase structure and greater crystallite size. This shows that the degree of crystallinity of anatase is pH-dependent, and lower acidity enhances the crystallinity, which also promotes the formation of large crystallite size. In another study conducted by

Mutuma et al. (2015), mixed phase (anatase and brookite) of TiO_2 calcined at 600 °C in a strongly acidic medium. While in the investigation reported by Cassaignon et al. (2007), a rutile crystalline phase was formed at the pH conditions less than 4.5, and only anatase structure formed at pH greater than 4.5.

Although the possibility of obtaining anatase structures in acidic medium is apparent. However, investigation of TiO_2 nanoparticles synthesized by a facile solgel method under acidic and basic media is necessary. This is because this will go a long way in exploring the microstructure and optical properties of TiO_2 nanoparticles produced.

Synthesis and mechanism reaction of ZnO

Zinc oxide is a white-yellowish crystalline substance soluble in both acid and base. It has attracted the interest of researchers due to its strong activity. ZnO agglomerates in water due to its polarity which could lead to deposition. It exhibits three highly crystalline forms, namely: zinc blende, wurtzite, and rock salt (Sirelkhatim et al. 2015). The wurtzite structure is the most common and stable form of zinc oxide at room conditions. At high pressure, ZnO transforms to rock salt phase. This oxide has a small covalent property and a very strong ionic character. The crystals of ZnO are depicted in Fig. 5, and the gray and yellow-shaded spheres signify Zn and O atoms, respectively.

Various approaches for the synthesis of ZnO nanomaterials can be categorized into a solution and vapor-based techniques. Among these methods, the solgel method is found to offer better control of the size and distributions of the nanomaterials. As-obtained ZnO nanomaterials can be prepared either at the pilot or at the laboratory plant scale. Synthetic methods have to do with the zinc precursors, precipitating agent, unit and process conditions which occur in four stages, namely, solvation, hydrolysis, polymerization, and transformation. According to scholars, physical and chemical parameters such as solvent types, pH, precursors, and temperature affect the morphological structures and the sizes of ZnO nanoparticles. Examples of precursors used are zinc acetate dihydrate, zinc nitrate hexahydrate, zinc chloride, zinc sulfate, and zinc acetylacetonate. The commonly used precursors are zinc acetate dihydrate and zinc nitrate hexahydrate. The reaction mechanism for the synthesis of ZnO nanomaterials is controlled in a basic medium using these precursors as initial materials which is shown in Fig. 6.

Zinc hydroxide is produced in both steps, and upon heating, ZnO is produced. This zinc hydroxide separates into Zn^{2+} and OH^{-}, followed by polymerization of hydroxyl complex to yield Zn–O–Zn which finally converted to ZnO. Thermochromism is a unique property of ZnO during synthesis which is the change of color as a result of a change in temperature. The color of ZnO changes from white to yellow at temperatures above 400 °C and becomes

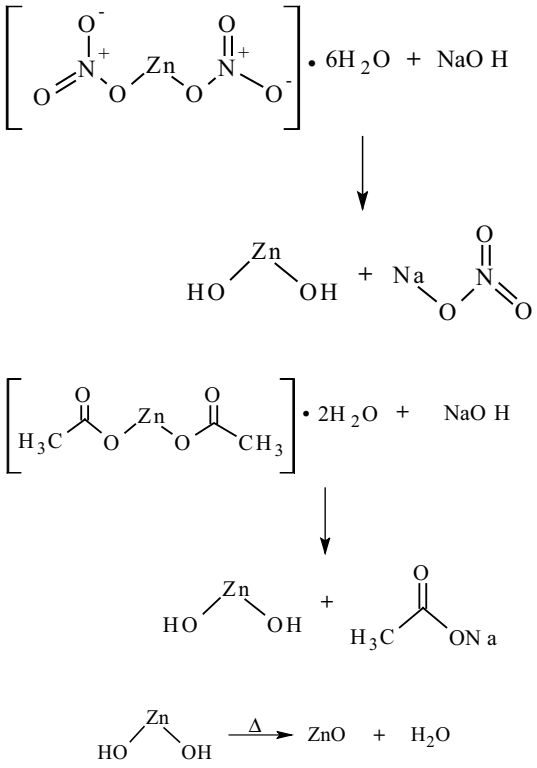

Fig. 6 Reaction mechanism of ZnO for the synthesis of ZnO

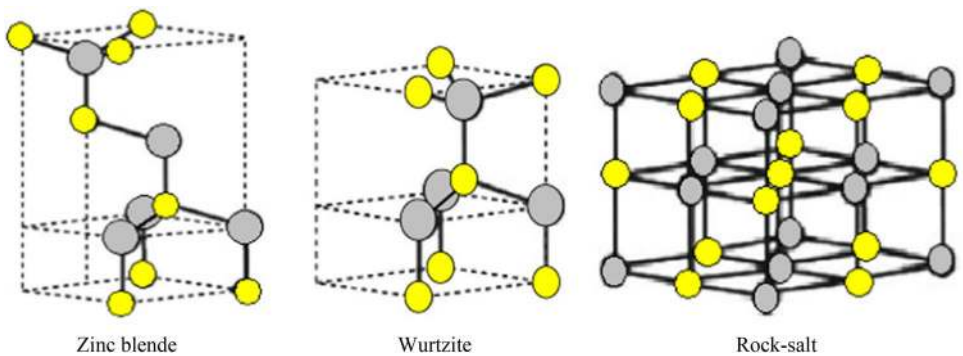

Fig. 5 Different forms of ZnO crystals

white on cooling. This could be as a result of the formation of crystalline lattice due to loss of oxygen.

The use of different precursors, variation in temperature and calcination temperature, pH, and organic solvents has been employed in studies for producing ZnO nanomaterials with unique properties using the solgel method. Bhardwaj et al. (2018) synthesized ZnO nanoparticles using $Zn(CH_3COO)_2{\cdot}2H_2O$ and KOH. The solution was stirred to form a milky mixture, centrifuged at 3000 rpm and then dried at 80 °C for 6 h. This synthetic approach for the production of ZnO nanoparticles was relatively different from the method used by Shaban et al. (2018). The precursor, organic solvent, and stabilizer used are zinc acetate [$Zn(CH_3COO)_2{\cdot}2H_2O$], 2-methoxy ethanol ($C_3H_8O_2$), and monoethanolamine (C_2H_7NO), respectively. The effects of precursor concentration and pH were investigated on the resultant solution. Oven-drying was done at 60 °C for 2 h, and it was allowed to age for 24 h at room temperature. Similar precursor and stabilizer but a different organic solvent were employed in the study reported by Aryanto et al. (2017). In their study, $Zn(CH_3COO)_2{\cdot}2H_2O$, C_2H_5OH, and C_2H_7NO mixture was stirred at ambient temperature with a magnetic stirrer for 1 h.

Acosta-Humánez et al. (2015) prepared ZnO by solgel method using $Zn(NO_3)_2{\cdot}6H_2O$ as the precursor and citric acid ($C_6H_8O_7{\cdot}H_2O$) as a complexing agent. This was conducted at 70 °C with vigorous stirring until a gel was obtained. This gel was calcined at 130 °C for 12 h. Mohan and Renjanadevi (2016) synthesized ZnO using $ZnSO_4{\cdot}7H_2O$ as a precursor and NaOH as the precipitating agent. The mixture obtained was stirred for several hours. The white precipitate was filtered and washed with distilled water, calcined at 100 °C, and then ground to form a fine powder. The prepared ZnO powder obtained from the previous step was calcined at a temperature ranging from 500 to 900 °C at 200 °C interval. Akkari et al. (2017) prepared ZnO nanoparticles by dissolving zinc acetate in methanol with methanolic KOH solution under vigorous stirring. The resulting precipitate was washed with ethanol and then sealed in a container.

The resulting ZnO nanomaterials strongly had different physicochemical properties. Some of the factors that affect the physicochemical properties of the prepared ZnO nanoparticles were precursor types, temperature, and pH. The effect of pH in the acidic medium resulted in non-uniformity and agglomeration of ZnO but as the pH increased giving rise to an alkaline solution, there was significant growth of ZnO nanocrystallites (Shaban et al. 2018). Increase in the precursor concentration affected the Zn–O bond length in the range of 1.9651–19,745 Å as reported by Aryanto et al. (2017). They confirmed that there was an increase in the lattice volume of the ZnO nanomaterial.

The particle sizes of ZnO nanomaterials increased with an increase in calcination temperature (Kayani et al. 2015). Likewise, Thirumavalavan et al. (2013) revealed that the nano-ZnO increased as the calcination temperature increased. In addition, they found that surface areas of the nano-ZnO at various temperatures are reduced, and their crystal sizes became agglomerated. They further gave explicit explanations on this effect viz, (1) particle size broadening was as a result of the morphological diffracting domain within the grains, and (2) the microstrain broadening was due to disparity in the *d*-spacing by odd crystalline stresses. In the ensuing section, the characterization, experimental conditions, and crystallite sizes of synthesized ZnO nanoparticles using solgel are presented in Table 3.

Characterization of TiO_2 and ZnO

TiO_2 and ZnO nanoparticles are characterized based on the purpose for which they are produced. This section gives the overview of different characterization techniques for morphological, structural, particle size, and surface area studies of TiO_2 and ZnO nanoparticles. These include the use of electron microscopy (SEM), transmission electron microscopy (TEM), X-ray diffraction (XRD), Fourier transform infrared spectroscopy (FTIR), Brunauer–Emmett–Teller (BET), X-ray photoelectron spectroscopy (XPS), dynamic light scattering (DLS), photoluminescence (PL), and ultraviolet–visible (UV–Vis).

SEM

SEM is a technique that provides information on the particle size, shape, and surface morphology of powdered sample but offers limited information on size distribution. The use of SEM has the disadvantages of time consumption and high cost. However, its major advantage is that easy sample preparation is needed. The SEM images in Fig. 7a and b signify the hexagonal wurtzite structure of ZnO nanoparticles. It was observed that at low calcination temperature, the particles formed were clusters, but particles of better morphology were obtained as the temperature of calcination increased. Likewise, at high temperature, less agglomeration was observed and the particles changed to the spherical nanocrystals in the range of 20–80 nm in diameters. The authors failed to give reliable information on this disparity of their findings. This is because the differences in their morphologies could be a result of weak physical forces in the synthesized ZnO nanoparticles.

The SEM micrographs of the TiO_2 nanoparticles at different calcination temperatures are depicted in Fig. 8. The scholars observed that the higher the calcination temperature, the larger the particle sizes. At the highest calcination temperature, grain boundaries were clearly observed. At

Table 3 Summary of as-synthesized ZnO nanoparticles via solgel methods from 2013 to 2018

Crystallite size (nm)	Characterization	Raw material	Condition	References
12–30	XRD, AFM	Zinc acetate dihydrate, ammonia hydroxide, methanol	pH 9 and 11, Calcination temperature of 500 °C	Abdullah et al. (2017a, b)
–	XRD, SEM–EDS, RAMAN, UV–Vis	Zinc acetate, sodium hydroxide	Temperature of 450 °C	Zargar and Arora (2017)
17	XRD, UV–Vis, FESEM	Zinc acetate dihydrate, sodium hydroxide, isopropyl alcohol, ammonia solution	pH 9, calcined at 200 °C, solvent ratio	Davis and Singh (2016)
49–200	XRD, FESEM	Zinc acetate dihydrate, methanol, sodium hydroxide	pH 9, calcined at 800 °C, the aging time of 4–24 h	Harun et al. (2016)
19.8	XRD, TEM	Zinc acetate dihydrate, oxalic acid, ethanol	Molar ratio precursor to water, calcination temperature of 400–600 °C, pH 2	Chung et al. (2015)
32–128	XRD, SEM, UV–Vis	Zinc acetate, sodium hydroxide	Calcination temperature of 100–700 °C	Shaikh et al. (2016)
20–30	XRD, SEM	Zinc acetate, methanol	Heat treatment at 400 °C	Shastri et al. (2014)
18.9	TGA, XRD, FESEM, UV–Vis, BET, XPS	Zinc acetate, oxalic acid	Calcination temperature of 400 °C, pH 2	Ba-Abbad et al. (2017)
8–100	XRD, TEM	Zinc acetate, polyethylene glycol, ethanol, ammonia	pH 5.5–8.5, molar ratio, temperature of 800 °C	Jin et al. (2014)
20–140	XRD, SEM, TGA	Zinc acetate dihydrate, oxalic acid, ethanol	Calcined at 400 °C	Yusoff et al. (2017)
20–30	XRD, SEM, EDAX	Zinc nitrate, zinc chloride, sodium hydroxide	Temperature at 100–200 °C	Preethi et al. (2016)
27	XRD, FESEM, EDS, FTIR	Zinc acetate dihydrate, ethylene glycol, ammonia solution	pH 6, calcined at 450 °C	Assi et al. (2017)
36	XRD, FTIR, BET, FESEM, EDX	Zinc acetate dihydrate, oxalic acid, ethanol	Calcination temperature of 400 °C	Kadhim and Bin-Ab-Rahim (2017)
21–84–40	XRD, FTIR, RAMAN, UV–Vis, FESEM, EDAX	Zinc acetate, ethanol, sodium hydroxide	pH 8, annealed at 500 °C	Manikandan et al. (2017)
31–53	XRD, SEM, UV–Vis, FTIR, EDX, PL	Zinc acetate dihydrate, citric acid	Calcination temperature of 400–600 °C	Hedayati (2015)
32	XRD, SEM–EDS, UV–Vis	Zinc acetate dihydrate, citric acid, ammonia solution	Calcined at 600 °C	Khan et al. (2013)
28	XRD, UV–Vis, TEM, RAMAN, PL	Zinc acetate, methanol, ethyl ethanol	–	El-Ghoul et al. (2015)
36.1	XRD, SEM UV–Vis	–	–	Ansari et al. (2015)
18	XRD, SEM, EDX, UV–Vis	Zinc acetate, methanol, trisodium citrate	Annealed at 450 °C	Brintha and Ajitha (2015)
19.3–83.6	AAS, FESEM, EDAX, XRF, XRD, TEM, DLS	Alkaline batteries, nitric acid, hydrogen peroxide, starch, dextrose	Calcination temperature of 400–800 °C	Díaz-de-León et al. (2017)
47.55–51.23	TGA, XRD, FTIR, FESEM, DRS, UV–Vis	Zinc acetate dihydrate, isopropanol, monoethanol amine	Annealed at 350–450 °C	Habibi and Karimi (2014)
10.05–19.2	XRD, SEM, FTIR	Zinc chloride, ethanol, sodium hydroxide, potassium hydroxide	–	Vanaja and Rao (2016)
> 80	XRD, ESEM	Zinc acetate dihydrate, isopropyl alcohol, triethyl acetate, sodium hydroxide	pH 2–10	Ashraf et al. (2013)
58.3	XRD, FTIR, SEM, Uv–Vis	Zinc acetate dihydrate, sodium hydroxide	–	Alwan et al. (2015)

Table 3 (continued)

Crystallite size (nm)	Characterization	Raw material	Condition	References
3–25	XRD, SEM, TEM, FTIR, TGA, DSC, UV–Vis	Zinc acetate dihydrate, sodium hydroxide	Stirring time of 500–2000 rpm	Khan et al. (2016)
18–34.7	TGA, XRD, BET, FTIR, FESEM, DRS, EDX	Zinc acetate, oxalic acid, ethanol, hydrochloric acid, ammonia solution	Molar ratio, pH 1–5, calcination temperature of 400–600 °C	Ba-Abbad et al. (2013)

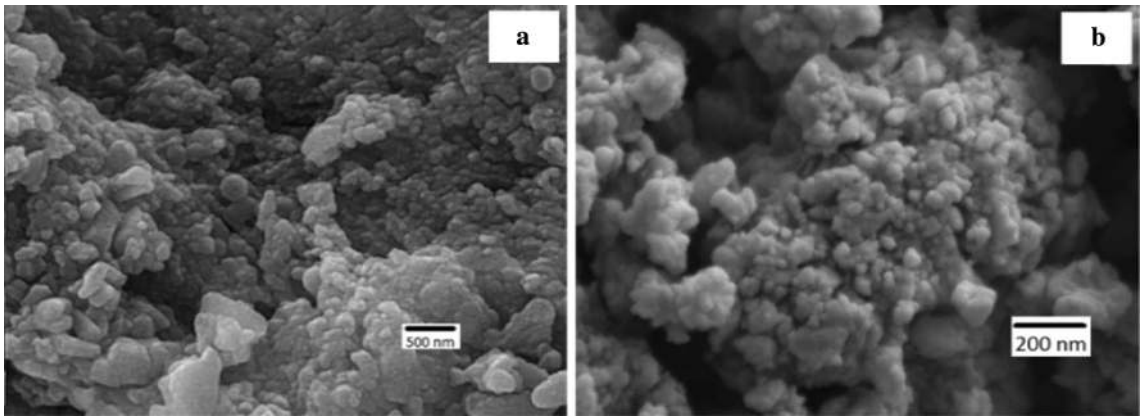

Fig. 7 SEM image of prepared ZnO nanoparticles **a** as-synthesized **b** calcined at 500 °C for 3 h (Jurablu et al. 2015)

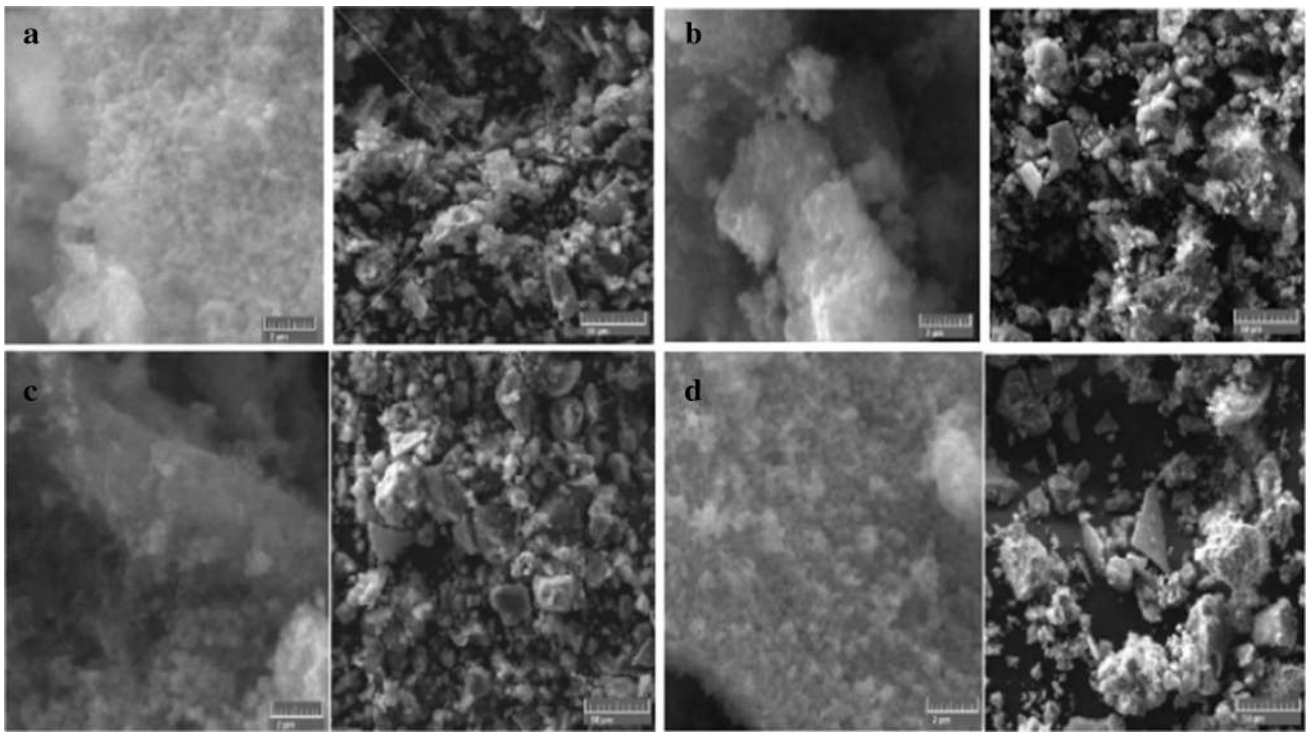

Fig. 8 SEM images of TiO_2 at calcination temperature, **a** 300 °C **b** 500 °C **c** 700 °C **d** 900 °C (Yudoyono et al. 2016)

300–700 °C, crystalline sizes of anatase and brookite TiO_2 nanoparticles were 10–18 nm and 4–13 nm, respectively. This appears that the higher the calcination temperature, the higher the grain size.

TEM

The TEM provides information on the morphological, surface behavior, and lattice fringes of nanomaterials. High-resolution transmission electron microscopy (HRTEM) can give information on the porosity and structural defects within crystals and crystallinity. The operating system is quite different from SEM; hitherto, it produces a similar type of information. Images generated by HRTEM are different from those of the high-resolution scanning electron microscopy (HRSEM). On the other hand, the energy-dispersive X-ray (EDX) combined with this equipment (HRTEM) provides the information on the elemental constituents of the nanomaterials. Importantly, EDX explains the effects of some parameters such as calcination temperature, pH, and aging time on the equivalent elemental compositions of the nanoparticles. Figures 9 and 10 show the TEM images of ZnO and TiO_2 nanoparticles annealed at different temperatures. Figure 18 images revealed that ZnO nanoparticles prepared at calcination temperatures of 500–600 °C gave a high magnification of HRTEM image of the ZnO nanoparticles. The synthesized nanoparticles are spherical, lattice fringes space of 0.24 nm, and the average particle size increased with an increase in the calcination temperature.

The TEM analysis of the synthesized TiO_2 nanoparticles at the various experimental conditions: pH, drying, and calcination temperatures, was studied by EL-Mekkawi et al. (2017). It was established that as the temperature gradually increased from 450 to 650 °C as depicted in Fig. 10, the predominant TiO_2 phase was anatase in a mixture of anatase and rutile phases. Phase transformation of the nanoparticles

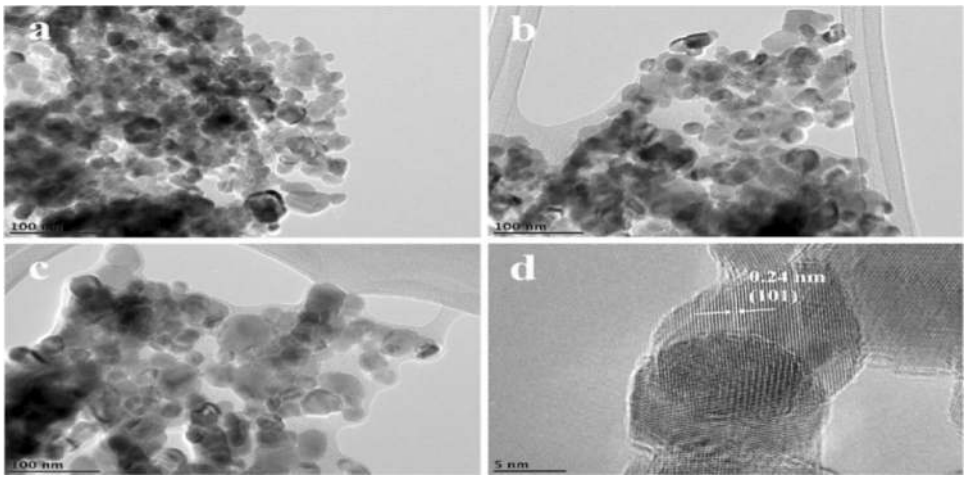

Fig. 9 HRTEM images of ZnO nanoparticles at **a** 500 °C, **b** 600 °C and **c** 700 °C as well as **d** high magnification of the ZnO (Golsheikh et al. 2017)

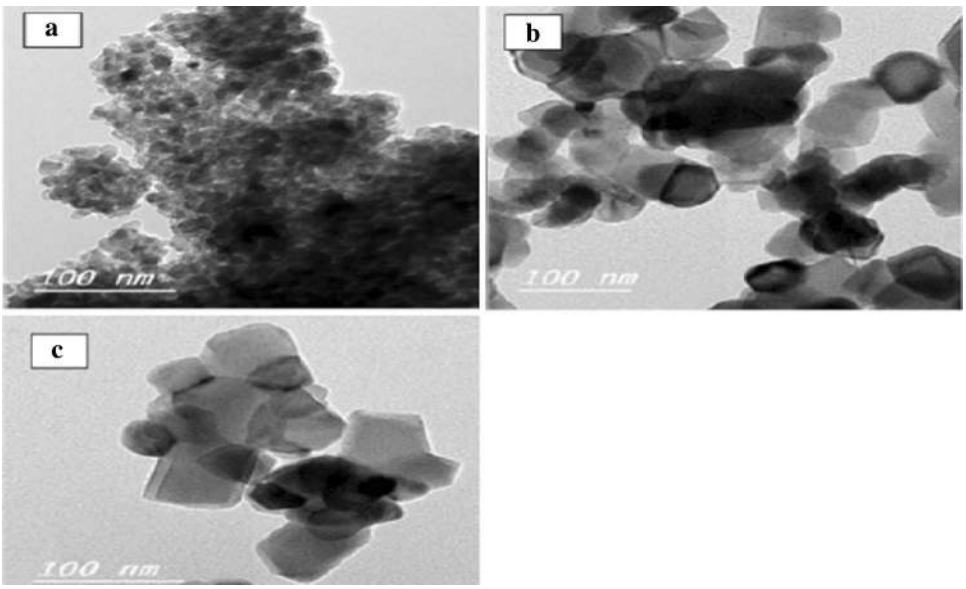

Fig. 10 TEM patterns of TiO_2 nanoparticles at calcination temperature **a** 450 °C **b** 550 °C **c** 650 °C (EL-Mekkawi et al. 2017)

was not only affected, and the degree of crystallinity and size distribution also slightly changed. The measured particle sizes of the synthesized TiO_2 at 450 °C, 550 °C, and 650 °C ranged from 5 to 25, 35 to 70, and 40 to 120 nm, respectively. The authors clearly pointed out that as the temperature increased crystallite size and phase ratio were influenced.

XRD

XRD is a rapid characterization method for identification of a phase of crystalline material. In this case, diffraction peaks are obtained. It helps to provide information on unit cell dimensions of nanomaterials: interatomic distance and angle of the atom. This analysis also gives a rough estimate of crystallite size through Debye–Scherer formula. It is invaluable for a successful structural characterization of nanomaterials in both single and multiphase. Figure 11 reveals the XRD patterns of as-prepared ZnO nanoparticles at different calcination temperatures as described by Golsheikh et al. (2017). The authors declared that the wurtzite phase of ZnO nanoparticles was indexed and the average crystallite sizes of the nanoparticles at 500, 600, and 700 °C were 15, 18, and 22 nm, respectively. It was established that as the calcination temperature increased the peak intensities and crystallite sizes also increased.

The X-ray diffractograms of TiO_2 nanoparticles calcined at 400 °C and 500 °C are shown in Fig. 12 as studied by Romeiro et al. (2017). They demonstrated that the prominent peaks at Bragg's angle of 25° signify the anatase phase while small amounts of rutile was also observed at other diffraction angles. Using the Scherrer equation, the scholars came up with the crystalline sizes of 10.5 and 19.6 nm for the synthesized nanoparticles at 400 and 500 °C, respectively.

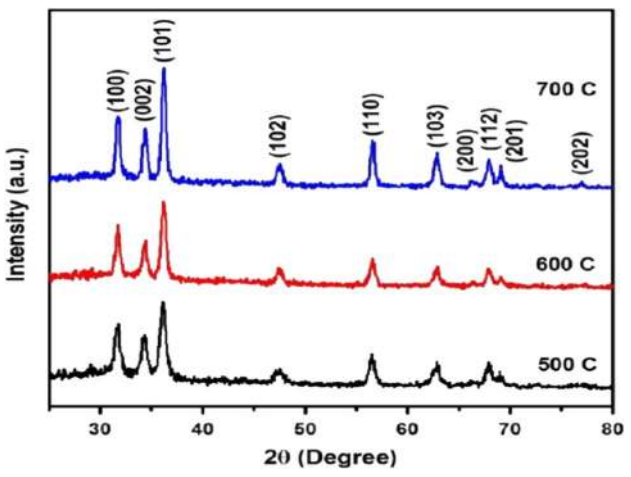

Fig. 11 XRD patterns of ZnO nanoparticles prepared using different calcination temperature: **a** 500, **b** 600 and **c** 700 °C (Golsheikh et al. 2017)

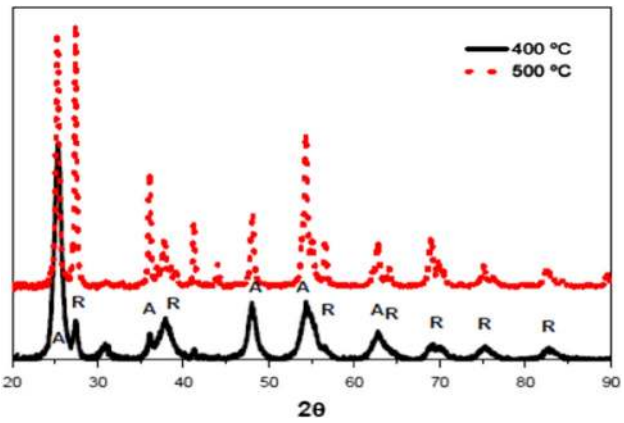

Fig. 12 X-ray diffraction patterns of anatase (*A*) and rutile (*R*) phases of TiO_2 nanoparticles at 400 °C and 500 °C

A similar finding was reported by Haider et al. (2017) on the prepared TiO_2 nanoparticles by solgel method calcined at different temperatures. They went further to explain the transformation of the TiO_2 phase. It was also established that the particle size of the anatase phase became smaller than other TiO_2 phases at low calcination temperature due to aggregation of the nanoparticles. However, the formation of anatase TiO_2 at low temperature could be as a result of high cell lattice energy involved in the calcination and growth coupled with bond breaking and reformation.

Some other analytical techniques

The large surface area of nanomaterials plays a vital role during applications. BET analysis is known to be the best method to determine the surface area of nanomaterials. This technique is based on adsorption and desorption theory and possible types of adsorption isotherms are Type-I, Type-II, Type-III, Type-IV, and Type-V. Most often, the Type-V is very similar to Type-IV and is not applicable to BET.

Golsheikh et al. (2017) synthesized TiO_2 nanoparticles and obtained the BET surface areas under different temperatures of 300, 600, and 700 °C as 26.7, 19.7, and 14.8 m^2/g, respectively. A previous study on ZnO doped with CuO nanoparticles annealed at the temperature range of 250–550 °C showed that remarkable decreases in surface areas were observed with a decrease in pore volumes and increase in pore diameter (Modwi et al. 2016). During their investigation, the obtained isotherms for pure ZnO and doped ZnO calcined at 550 °C were similar. A plausible reason could be that clogging pores resulted from aggregation at high temperatures. Following the opinion of different scholars, multi-element-doped TiO_2 via solgel method was calcined at 200, 300, and 400 °C by de-Luna et al. (2018), and they found that the decrease in the specific area (204.23 to 127.31 m^2/g), increase in average pore

size (7.79 to 10.99 nm), and decrease in volume (0.40 to 0.35 m^3/g) were due to pore blocking during the N_2 gas adsorption–desorption isotherm. Also, the synthesized TiO_2 nanoparticles at pH 8 and calcination temperatures of 300–800 °C (Khan 2017) and TiO_2 samples calcined at 350–600 °C (Fu et al. 2017) gave similar trends. Therefore, the findings of different scholars signify that these nanoparticles, when subjected to intense calcination temperatures tend to have lower surface areas due to the crumbling of pores.

FTIR and Raman spectroscopies are used for vibrational information of nanoparticles. They provide information on the fingerprint regions of chemical bonds in molecules. In this context, FTIR spectra of synthesized ZnO and TiO_2 nanoparticles calcined at different temperatures by a solgel technique using zinc acetate dihydrate and titanium isopropoxide as their precursors have been provided (Kayani et al. 2015; Fernández-Catalá et al. 2017). Figure 13 depicts the FTIR spectra of ZnO nanoparticles calcinated at 300–750 °C. The strong peaks of C=O and O–H stretching modes of vibration gradually diminished at high temperatures. The ZnO peak appears between 435.06 and 413.36 cm^{-1} and became sharpened indicating an increase in the crystallinity of nanoparticles as the temperature increased.

The FTIR spectra of the TiO_2 samples prepared at 250–900 °C by Fernández-Catalá et al. (2017) were analyzed as shown in Fig. 14. The broad bands at 3000 to 3500 cm^{-1} and 1600 cm^{-1} were attributed to the OH stretching of physisorbed water on the surface of TiO_2. As the calcination temperature increased, the OH band diminished in intensity, signifying the loss of the physisorbed water on the TiO_2 surface. As such, the weakness in the Ti–OH vibration bands during calcination according to them might be detrimental to its applications industrially.

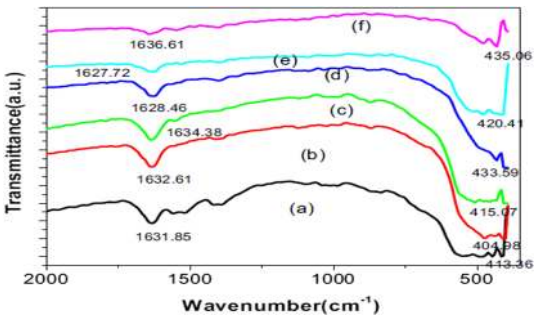

Fig. 13 FTIR spectra of wurtzite nanoparticles (**a**) before and after calcinated temperature at **b** 300 °C, **c** 500 °C, **d** 650 °C, **e** 700 °C, and **f** 750 °C (Kayani et al. 2015)

Adsorption activity of ZnO and TiO_2

Numerous adsorbents have been developed for the treatment of pollutants, but they are associated with certain drawbacks. Owing to the properties such as surface area, porosity, site density and crystallinity of TiO_2 and ZnO, these photocatalysts have been recognized to be effective in removing heavy metal cations and organic pollutants from aqueous solutions. Additionally, pore size and surface chemistry govern the adsorption capability of nanomaterials. Porous nanomaterials are generally categorized into microporous (< 2 nm), mesoporous (2–50 nm) and macroporous (> 50 nm) as defined by the International Union of Pure and Applied Chemistry (IUPAC). The microporous sizes of TiO_2 and ZnO nanoparticles help to perfect the adsorption and separation techniques using these oxide nanoparticles, while the use of meso- and microporous nanomaterials would ease mass transfer.

Basically, adsorption processes in wastewater using TiO_2 and ZnO as shown in Fig. 15 can be divided into physisorption (physical) and chemisorption (chemical). The degrees

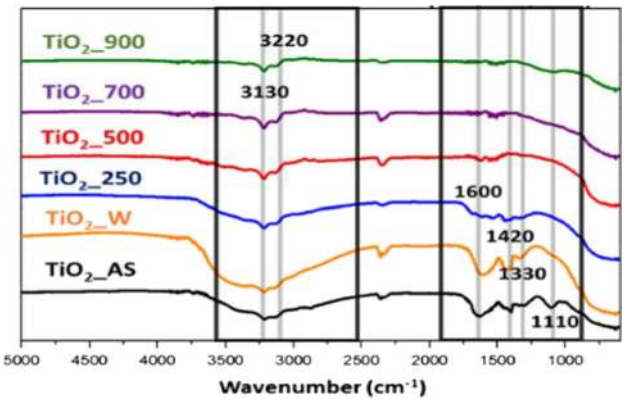

Fig. 14 FTIR spectra of TiO_2 nanoparticles calcined at 250–900 °C (Fernández-Catalá et al. 2017)

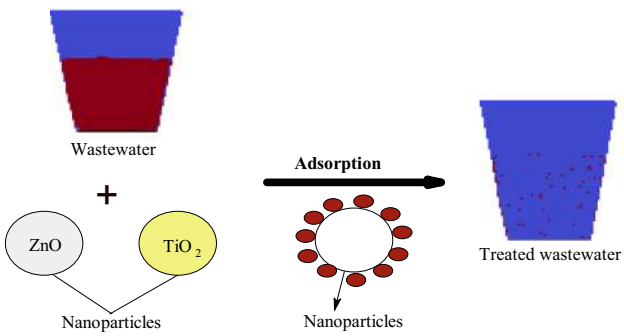

Fig. 15 Adsorption process using nanoparticles

of the two types of adsorption are influenced by weak intermolecular interactions like London van der Waals forces, hydrogen bonding, covalent bonding, electrostatic interaction, dipole–dipole interaction, polarity, and hydrophobicity. On the other hand, ion exchange between sorbents and sorbates occurs in chemisorption.

TiO_2 and ZnO as adsorbents for water treatment have been pointed out to be advantageous due to the high adsorption capacity and great affinity for pollutants. They are perhaps the most promising nanomaterials for water treatment. However, of particular interest, is the fact that certain circumstances during the time of applications of these nanomaterials occasionally render them ineffective. Thus, interests should be developed toward incorporating TiO_2 and ZnO into natural materials like clay for the development of nanocomposites in order to increase their interfacial interactions and overcome the problems of recycling after treatment.

Clay as natural adsorbents

Clays are indispensable nonpolluting natural materials and their wide ranges of applications include polymer, water, cosmetics, ceramics, paints, pharmaceutical, pulp, and paper industries. Depending on academic contexts, clays are referred to as natural by occurring fine particles composed of fine-grained and crystal minerals such as silicon oxide, carbonates, and metal oxides, which become harden when fired. The components in clay are in different structural layers and compositions as a result of their polytypic and structural arrangements called polytypism. Clay minerals are hydrous aluminosilicates that can retain large amounts of water with other properties such as colloidal behavior, swelling, and adsorption capacities. The clay minerals are classified into kaolinite, illite, montmorillonite (smectite), and chlorite (Adeyemo et al. 2015).

The kaolinite, montmorillonite, illite, and bentonite are commonly used because they exhibit high surface area, availability, stability, and structural characteristics. These minerals are found to be naturally abundant, non-toxic, and have significant roles in scavenging pollutants in wastewater either via ion exchange or adsorption processes or both. Hence, they are basically used as depolluting agents.

The adsorption processes which occur on the solid surface in contact with ionic solution involves the adsorption of ions called potential determining ions which gives the surface either positive or negative charge with respect to the charge originated from the crystal lattice. The layer which comprises double (negatively charged) and the edge double layers that are amphoteric (either negatively or positively) charged depends on the composition of the aqueous solution. Notably, the adsorption processes are cation exchange adsorption on the surface layers and the chemisorption of anions at the edge surfaces. The ensuing sections will focus on the application of these clay minerals and their composites in the treatment of wastewater.

Forms of clay minerals

Kaolinite

Kaolinite group is classified as 1:1 type layer silicates with a tetrahedral layer of silica (SiO_4) joined together with an oxygen atom and an octahedral sheet of alumina (AlO_6). Figure 16 describes the structure of kaolinite, and it possesses high chemical stability, low expansion, and cation exchange capacity. The kaolinite group is structurally divided into dioctahedral and trioctahedral minerals (Uddin 2016). The dioctahedral minerals include kaolinite, dickite, nacrite, and halloysite, while the trioctahedral minerals comprise the antigorite, chrysotile, chamosite, and cronstedite, with a general formula of $Al_2Si_2O_5(OH)_4$ and theoretical structural composition of 46.54% SiO_2, 39.50% Al_2O_3, and 13.96% H_2O. The mentioned subgroups of this clay mineral consist of silicate sheet (Si_2O_5) bonded to aluminum hydroxide [$Al_2(OH)_4$] known as the gibbite layer. There are no interlayer swelling and charges. The kaolinite, dickite, and nacrite are polytypes which occur as plates, while the halloysite is the hydrated polymorph that is tubular in shape.

The clay mineral that is rich in kaolinite is called kaolin. Kaolin is a soft and whitish powder; it has a melting point of 1750 °C. It is naturally found together with other minerals such as muscovite, feldspar, quartz, and anatase. Structural transformations occur upon thermal treatment of the kaolinite group in the air at atmospheric pressure. At 100 °C, the water in the kaolin is dried off and the end state is called leather dryness. Bone dryness is observed at temperatures between the range of 100 °C and 550 °C. Endogenic dehydration of kaolin starts from 550 to 600 °C to produced metakaolin, $Al_2Si_2O_7$, but the continuous loss of hydroxyl

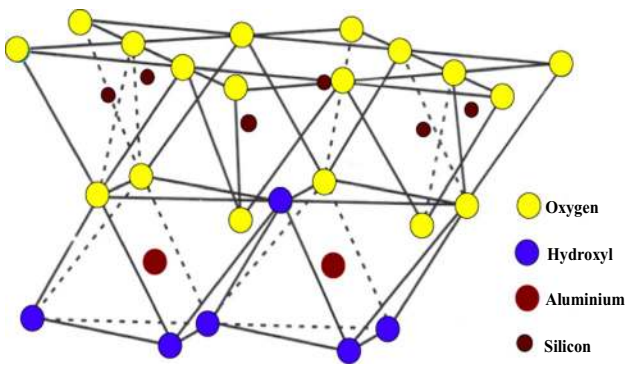

Fig. 16 Structure of kaolinite

(dehydroxylation) is achievable at 900 °C. Further application of heat transforms the metakaolin to aluminum–silicon spinel, $Al_4Si_3O_{12}$ (at the temperature of 925–950 °C), and then finally to platelet and needle mullite, upon calcination at the temperature of 1050 °C to 1400 °C.

Montmorillonite

Montmorillonite believed to be smectite is a 2:1 phyllosilicate mineral consisting of two tetrahedral silica sheets and an octahedral sheet of alumina (Brigatti et al. 2013). The structure of montmorillonite as presented in Fig. 17 allows the passage of water causing swelling and cation exchange ability. The cation exchange capacity is as a result of the replacement of Mg for Al leaving the neighboring oxygen atoms negatively charged. On the application of heat to this type of clay, it changes to arcillite. Montmorillonite has been reported to be cheap and is used for the adsorption of contaminants (Yuan et al. 2013).

Illite

Illite is a 2:1 type of clay mineral with tetrahedral silica (T) and octahedral layers (O). It is a silica–gibbsite–silica sandwich (T–O–T). The structure illite as exemplifies in Fig. 18 includes phengite, celadonite, hydrous micas, brammallite, and glauconite. The negative charge on the surface layers is as a result of the replacement of aluminum for silicon in the tetrahedral sheet. The balancing charge comes from potassium as shown in Fig. 18, and possible balancing cation could be from cesium and ammonium (Mukherjee 2013). The presence of these interlayer cations makes illite clay to be nonexpanding, disallowing the incorporation of water molecules into its structure.

Characteristics common to clays

The features of clay minerals strongly depend on their chemical compositions, sizes, and surface layers. These characteristics allow more understanding of the nature of clay minerals. The common properties associated with clay are plasticity, surface area, and ion exchange capacity. Clays become plastic when combined with water and variations in plasticity are as a result of conserved interstitial materials during weathering. Shrinkage determines the plasticity of clay; the greater the shrinkage the more plastic a clay material. When fired, the new form of clay is achieved without any attempt to return to the original physical and chemical properties.

In general, the surface area enhances the adsorption capacities that result from the negative charge on the structure of clay mineral. Importantly, the sizes and charges of the cations of clay determine its swelling property. A swelling

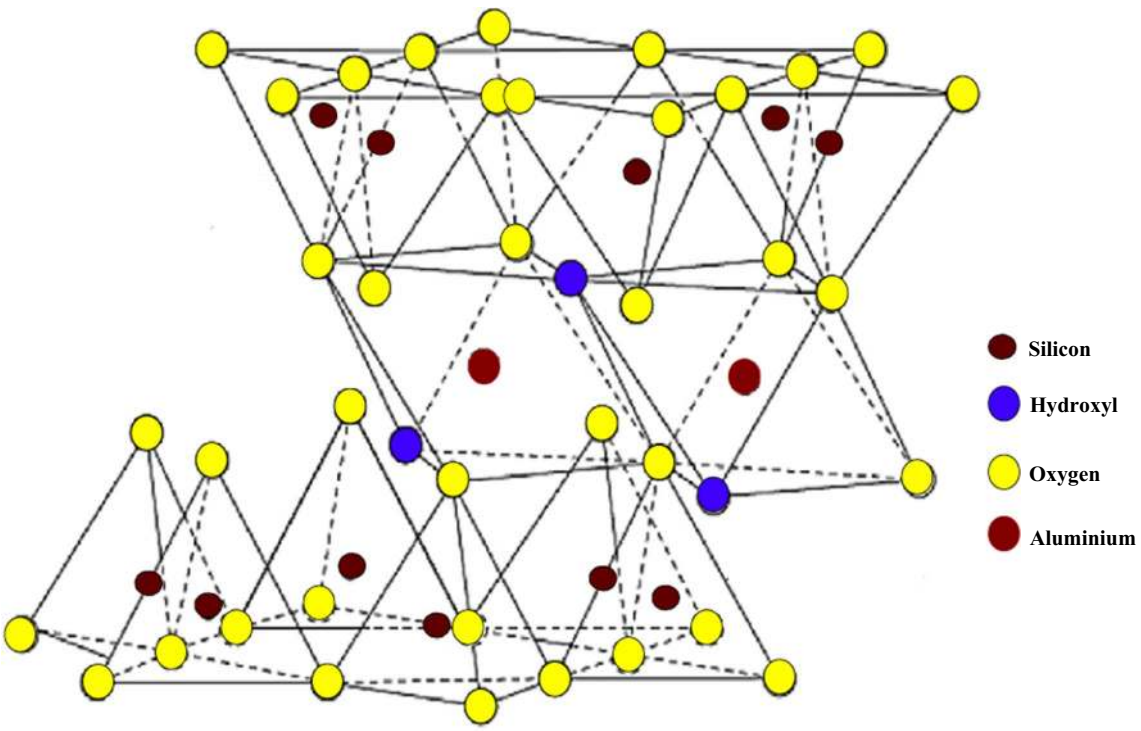

Fig. 17 Structure of montmorillonite

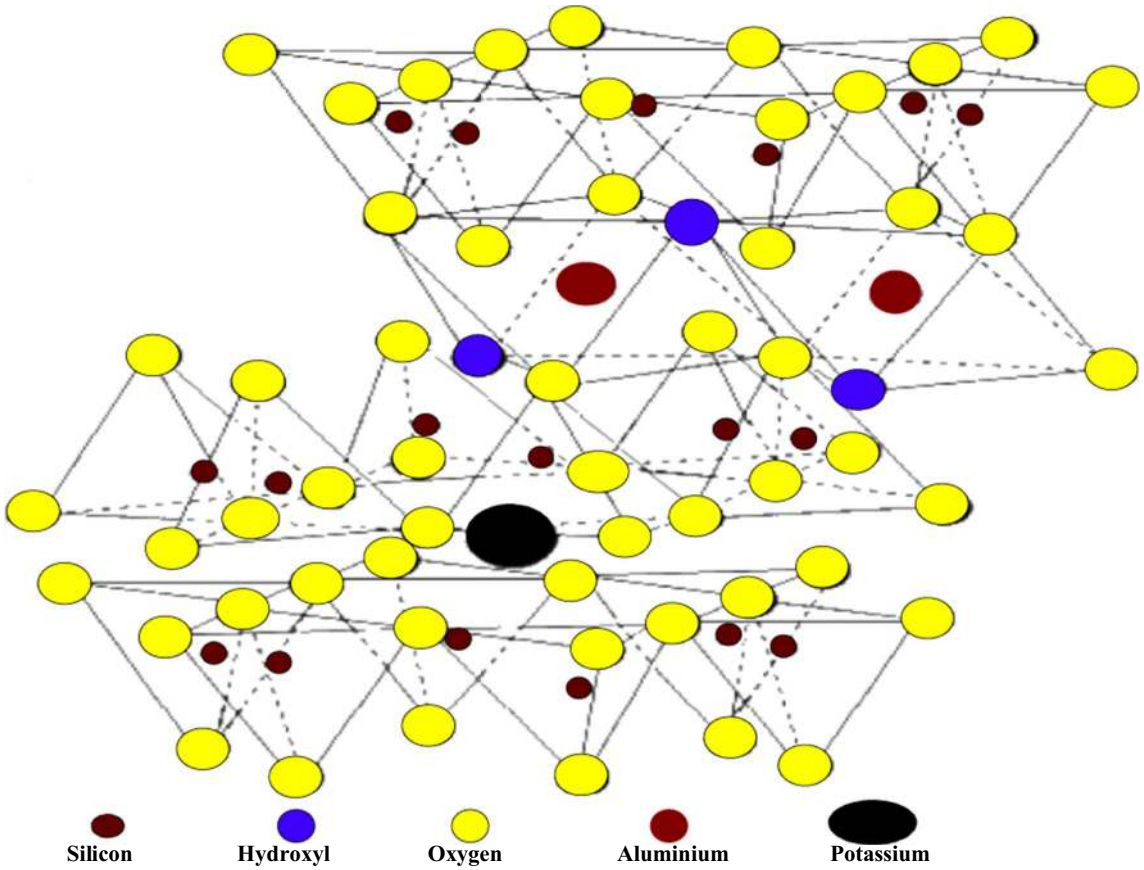

Fig. 18 Structure of illite

clay is that with the ability to retain water and expand upon hydration (Carrier et al. 2013, 2014).

Adsorption characteristics of clay minerals, clay/ZnO, and clay/TiO_2 nanocomposites

The chemistry of phyllosilicate in clays determines their adsorptive behavior, and their exchangeable cations, hydroxyl, and oxygen are responsible for their physical adsorption due to van der Waals interaction, chemisorption, and catalytic capacity. The adsorption ability of a given clay is explicitly explained under the influence of parameters like contact time, pH, initial concentration, dosage, and temperature. In this review, the literature of last 5 years (2013–2018) by various researchers in the use of clays, clay/ZnO, and clay/TiO_2 nanocomposites for the removal or degradation of contaminants from wastewater has been studied. This is because the comprehensive overview of these adsorbents and their adsorptive abilities for various pollutants is quite important.

Clays for wastewater treatment

The interests of scholars preferably using clay for removing pollutants from contaminated waters as shown in Table 4 have been in the used as adsorbents around the globe.

Nanocomposites like clay/TiO_2, clay/ZnO, and clay/TiO_2/ZnO are multiphase solid materials in nanosize explored as good adsorbents for water treatment. The formation of new materials with unique flexibility and improved properties such as affinity to contaminants, mitigate the release of nanoparticles, and enhanced strong antibacterial activity is a welcome idea. The development of nanomaterials that have been shown to possess most of these properties is attracting the attention of researchers. Thus, researchers have considered their applications to be important in the field of water sanitation.

Clay/TiO_2

The use of TiO_2 nanocomposites for the treatment of water has served as an alternative to that of commercial TiO_2 due to their high adsorptive properties, low cost, and

Table 4 Summary of the clay used for the removal of pollutants from wastewater

Adsorbent	Characterization	Experimental condition	Finding	Pollutant	References
Saudi Arabian clay	SEM, EDX	Initial pH	The significance of pH during the adsorption and desorption study	Heavy metals	Lukman et al. (2013)
Natural clay	SEM, EDX	Initial concentration, contact time, pH, temperature dosage	The rate of adsorption increased with increase in pH	Methylene blue	Mahammedi and Benguella (2016)
Algerian kaolin	XRD, BET, SEM	Contact time, initial concentration, pH, dosage, temperature	Experimental data favored Langmuir isotherm and pseudo-second-order kinetic	Tannery (acidic dye)	Zen et al. (2018)
Brazilian kaolin	XRF. XRD, BET, FTIR, SEM, TGA, DLS	Concentration	The adsorption system obeyed Elovich kinetic model and Langmuir model	Malachite green dye	Caponi et al. (2017)
Bentonite (Jeddah, Saudi Arabia)	XRD, BET, XRF	Temperature	Metal ion adsorption increased with an increase in temperature The adsorption process was found to be endothermic	Copper and nickel ions	Aljlil and Alsewailem (2014)
Sepiolite, kaolin and talc		Concentration, pH	The zeta-potential analysis showed that the adsorption capacity of the clay samples in acidic medium was higher than in basic conditions	Anionic reactive dye	Rahman et al. (2015)
Algerian kaolin	BET	Contact time, initial concentration, stirring speed, salt concentration, dosage	Dubinin–Radushkevich and Temkin models were found to be the best that fitted the adsorption process The thermodynamic study showed that the adsorption process was endothermic	Methylene blue	Rida et al. (2013)
Calcareous, smectitic clay	XRF	Initial concentration, contact time, pH, temperature	The pH and the presence of carbonate impurities affected abilities of the clay samples to remove the metal ions	Copper and zinc ions	Sdiri et al. (2014)
Kaolin	XRD, SEM	Reaction time, initial concentration	The experimental data fitted well for the Langmuir isotherm model	Dye	Hajjaji et al. (2016)
Organobentonite	XRD, SEM, BET, FTIR, Zeta-potential	pH, initial concentration	The Langmuir and pseudo-second-order models were favored The adsorption system was endothermic and spontaneous	Dye	Huang et al. (2017)

Table 4 (continued)

Adsorbent	Characterization	Experimental condition	Finding	Pollutant	References
Bentonite and kaolin		pH, dosage, ionic strength	The increase in pH and facilitate the removal of cationic xylan copolymer	Cationic polymer	Konduri and Fatehi (2017)
Algerian clay	XRD, SEM, FTIR	Initial concentration, pH, contact time, dosage	The pH value increased as the adsorption rate decrease The increase in surface area with an increase in adsorbent dosage enhanced the elimination of pharmaceutical pollution The Langmuir model was a better fit than the Freundlich model	Pharmaceutical (diclofenac and potassium)	Mabroukia and Akretchea (2015)
Organobentonite	BET, FTIR, SEM, XRD, potentiometer	pH, surface modification, initial concentration, contact time	The adsorption data follow the pseudo-second-order equation and Freundlich isotherm model	Basic dye	Anirudhan and Ramachandran (2015)
$Mg(OH)_2$/Algerian bentonite	XRF, XRD, TGA, BET, SEM, FTIR	Contact time, temperature, adsorbent dosage, ionic strength, initial concentration	The adsorption process was found to be physisorption, endothermic and spontaneous in nature	Reactive dye	Chinoune et al. (2016)
Modified kaolin	SEM, XRD, XRF, FTIR		Functional groups such as hydroxyl, ammonium and nitrate ions on the surface of kaolin were responsible for the adsorption of chromium The process of adsorption obeyed pseudo-second-order kinetic and Langmuir model The process was spontaneous and exothermic in nature	Chromium ion	Lin et al. (2014)
Kaolin		Initial concentration, contact time	The correlation coefficient depicted that Freundlich adsorption isotherm model was more favored than the Langmuir model	Nitrate	Mohsenipour et al. (2015)
Bentonite	XRD, BET, FTIR, TGA, XPS	Contact time, pH, initial concentration	The isotherm fitted well by Langmuir and Freundlich–Peterson models The adsorption occurred due to the interaction of silanol groups with anion and hydroxyl/sulfonic groups	Reactive dye	Aguiar et al. (2017)

Table 4 (continued)

Adsorbent	Characterization	Experimental condition	Finding	Pollutant	References
Natural clay (China)	XRD, SEM, XRF, FTIR, CEC, BET, zeta-potential analyzer	Agitation time, initial concentration, solution pH, adsorbent dosage	Adsorption process followed the pseudo-second-order kinetics and Langmuir model The adsorption capacity was attributed to its structure and surface properties	Ammonium ion	Alshameria et al. (2018)
Bentonite	FTIR, XRD	Shaking speed, pH, temperature, initial concentration, particle size	Harkin Jura was the most favored and the adsorption process follows pseudo-second-order kinetic Bentonite clay depicted the dual nature of exothermic and endothermic, spontaneous and non-spontaneous properties reflecting the effects of temperature on its adsorption capacity	Reactive black 5 dye	Amin et al. (2015)
Algerian clay	XRD, BET, ZetaPhoremeter	Contact time, initial concentration, pH, dosage and temperature	The adsorption process obeyed the Langmuir model and adsorption kinetic follows the pseudo-second-order model	Acid dye (derma blue R67)	Zen and El Berrichi (2014)

Table 5 Summary of the clay/TiO_2 nanocomposites used for the removal of pollutants from wastewater

Adsorbent	Characterization	Experimental condition	Finding	Pollutant	References
TiO_2/Tunisian clay	BET, XRD, FTIR, TGA	Oxidizing agent, initial concentration	High photodegradation was as a result of stability of the TiO_2 anatase phase Hydrogen peroxide serves as a promising oxidant for degradation of dye under UV	Anionic reactive dye	Bel-Hadjltaief et al. (2014)
TiO_2/Polish halloysite	XRF, XRD, TEM, FTIR, BET	Time	The presence of TiO_2 in the nanocomposites photodegraded aniline and chloro derivatives greater the commercial TiO_2	Chloroaniline	Szczepanik et al. (2017)
TiO_2/Montmorillonite	XRD, SEM, FTIR, BET, TG–DTA	Time	The TiO_2 nanoparticles had large photocatalytic activity and the adsorbent for environmental remediation such as regeneration possibilities	Methylene dye	Chen et al. (2014a)
TiO_2/Bentonite	XRD, BET	Time	The pollutants are removed via adsorption and photocatalyst	Anionic and cationic dye	Sahel et al. (2014)
TiO_2/WO_3/Bentonite	XRD, EDS, FTIR, BET, AFM, SEM	Time, initial pH, temperature, initial concentration	There was an increase in the specific surface of the nanocomposites compared to bare clay	Methylene dye	Yang et al. (2015)
TiO_2/Clay	XRD, FTIR, AFM, SEM	Time	The nanocomposites showed high crystallinity degree and surface for adsorption of methylene blue and simultaneous removal of pollutant matrix (MB and cadmium)	Methylene blue and cadmium	Guillaume et al. (2018)
TiO_2/montmorillonite	FTIR, TG–DTA, BET, XRD, SEM, EDX	Time	The synthesized nanocomposites exhibit good adsorption and photodegradation properties and recovery process	Dye	Djellabi et al. (2014)
TiO_2/bentonite	FTIR, SEM, XRD, BET	Temperature	The formation of hydroxyl radical from TiO_2 acts as an active site for a photocatalytic agent in the degradation process The adsorption of dye molecule in an aqueous phase fitted best for Langmuir isotherm model	Methylene blue and Rhodamine B	Laysandra et al. (2017)
TiO_2/clay	XRD, TEM, FESEM, FTIR, BET	Time	The photodegradation of methylene blue and chlorobenzene depend on the clay texture as well as the surface area	Methylene blue and chlorobenzene	Mishra et al. (2017)

Table 5 (continued)

Adsorbent	Characterization	Experimental condition	Finding	Pollutant	References
TiO_2/clay	SEM, XRD, TEM, EDX, BET	Time	The clay exhibited good support for TiO_2 nanoparticles which serve as excellent photocatalytic performance and regeneration study	Methylene blue	Wu et al. (2019)
TiO_2/sepiolite	HRTEM, XRD, FESEM, EDX, XPD	Time, pH	The nanocomposites have photocatalytic properties for the photodegradation of organic pollutants	Dyes	Liu et al. (2018)
TiO_2/kaolin	XRD, FTIR, SEM, EDX, BET	Time, calcination temperature, concentration	The nanocomposites calcined at lowest temperature have the best performance photocatalytic activity due to its high surface area and porosity The nanocomposites are recovered and reused for three consecutive cycles	Coomasie brilliant blue dye	da Silva Lopes et al. (2019)

regeneration possibilities. Table 5 shows the synthesis and characterization of clay/TiO_2 nanocomposites used for the removal/degradation of contaminants in wastewater.

Clay/ZnO

The advantages of embedded ZnO nanoparticles in or on the surface layers of clay for the formation of matrices are due to swelling, photocatalytic and ion exchange properties. Table 6 presents the synthesis and characterization of ZnO nanocomposites for adsorption and photocatalytic degradation of pollutants in wastewater.

Clay/TiO_2/ZnO

Only a few research studies have been done on the synthesis and characterization of TiO_2/ZnO/clay nanocomposites. Thus, to date, the synthesis and application of heterogeneous catalysts immobilized on clay are still being awaited. TiO_2/ZnO was anchored on Tunisia clay for the photocatalytic degradation of methylene green in water (Bel-Hadjltaief et al. 2016). The heterogeneous nanocomposites were characterized by SEM, HRTEM, and zero-point charge of pH (pHzpc). The working operations of the experimental setup were evaluated under the effects of catalyst dosage, pH, initial dye concentration, and UV irradiation intensity. They found that almost complete mineralization occurred at 30 min in the presence of the nanocomposites under UV irradiation, demonstrating a positive effect of ZnO nanoparticles in the catalytic process. In the study reported by Vaizoğullar (2017), the photocatalytic activities of TiO_2, ZnO, TiO_2/ZnO, and TiO_2/ZnO/sepiolite catalysts were determined. The composites were synthesized for the degradation of flumequine antibiotic. The photocatalysts were characterized by SEM, XRD, FTIR, and zero-point charge for their photocatalytic performance. The operating conditions which included pH, initial sorbate concentration, and dosage were investigated. It was reported that sepiolite and ZnO played a vital role in the adsorption and degradation of flumequine on the surface of the catalyst.

As reported by Huanhuan et al. (2018), a novel clay nano-based catalyst of ZnO/TiO_2/rectorite was synthesized and characterized for photodegradation and adsorption of methylene blue from the aqueous phase. The experiment was conducted by varying the conditions of the solution pH, catalyst dosage, and TiO_2 mass ratio. The study showed that the degradation kinetics of methylene blue obeyed the Langmuir–Hinshelwood model. They found that TiO_2 enhanced the photocatalytic activity of the nanocomposites in the removal of the dye, while ZnO/rectorite was responsible for both the photodegradation and adsorption processes.

Table 6 Summary of the clay/ZnO nanocomposites used for the removal of pollutants from wastewater

Adsorbent	Characterization	Experimental condition	Finding	Pollutant	References
ZnO/montmorillonite	XRD, FTIR, SEM	Time, initial pH, initial concentration	The degradation ability of the nanocomposites was almost two-third higher than ZnO	Phenol	Ye et al. (2015)
ZnO/montmorillonite	XRD, FESEM	Contact time, dosage, initial concentration, pH	The presence of ZnO nanoparticles increased the surface area resulting in a higher adsorption rate The regeneration of the nanocomposites after three times of use showed that the adsorbent still had adsorption capacity for divalent ions	Lead and copper ions	Sani et al. (2017)
ZnO/bentonite	XRD, SEM	pH, initial concentration, dosage	The nanocomposites effectively removed safranine dye and decrease TOC under sunlight irradiation Regeneration study indicated the advantage of the practical application of the nanocomposites due to its stability and reusability	Safranine dye	Sonawane et al. (2016)
ZnO/Fe_2O_3/rectorite	SEM, XRD, FTIR, TGA, BET	Dosage, time, initial concentration	The ZnO assisted in the removal of methylene blue with a proposed mechanism	Methylene dye	Wang et al. (2018)
ZnO/sepiolite	FTIR, XRD, SEM	Time, initial concentration	The nanocomposites had the surface area and functional groups capable of adsorbing the dye	Congo red dye	Vahidhabanu et al. (2017)
ZnO/bentonite	XRD, XRF, FTIR	Dosage, pH, initial concentration	The photodegradation increases with decreasing the dye concentration	Textile azo dye	Boutra and Trari (2018)
ZnO/bentonite	XRD, SEM	Time, pH	The radical oxidation reagents are responsible for photodegradation process	Ciproxin	Sponza and Oztekin (2015)
ZnO/clay	XRD, FESEM, TEM, FTIR, UV–Vis, TG–DTA, BET	Time	The ZnO/clay nanocomposites have better adsorption efficiency than ordinary ZnO nanoparticles	Methylene blue	Akkari et al. (2015)
ZnO/Fe2O3/sepiolite	FTIR, XRD, FESEM, EDX, TEM, TG, BET	Temperature, time	The nanocomposites decolorized methylene blue dye and maintained its photocatalytic activity after reuse in consecutive cycles	Methylene blue	Akkari et al. (2017)
ZnO/sepiolite	XRD, TEM, EDX, BET, SEM, FTIR	Time	The nanocomposites were used for the photodegradation of some emerging contaminants under solar light irradiation	Pharmaceuticals	Akkari et al. (2018)

Table 6 (continued)

Adsorbent	Characterization	Experimental condition	Finding	Pollutant	References
ZnO/clay	XRD, BET, FTIR, SEM, HRTEM, EDX	Time, pH, dosage, initial concentration, inorganic anions	The removal of dye via heterogeneous photocatalytic process under solar irradiation The nanocomposites have high recyclability	Dye	Bel-Hadjltaief et al. (2018)
ZnO/kaolin	PL, XRD, SEM	Concentration, dosage, pH	The nanocomposites act as photocatalyst in water purification under sunlight The nanocomposite catalysts were easily recovered through filtration and no significant loss in the adsorbent after successive cycles	2-Chlorophenol	Zyoud et al. (2019)

Antibacterial activity of clay/TiO_2, clay/ZnO, and clay/ZnO/TiO_2 nanocomposites

Microbes are pathogens that are a menace and lethal to human beings. Microbes such as virus, fungi, algae, protozoa, and bacteria cause waterborne diseases like dysentery, abscesses, diarrhea, and typhoid. Both natural and synthesized adsorbents have been developed in recent years including clay minerals, nanoparticles, clay-supported metal/oxide nanoparticles, and clay-based nanocomposites for the removal of microbial organisms from water (Annan et al. 2018). Method of adsorption for the removal of bacteria from water has been found not to produce by-products, making it a better advantage over other water purification methods.

As depicted in Fig. 19, Morrison et al. (2016) described the antimicrobial mechanism of Oregon Blue clays. They opined that interlayer cation exchange, pyrite oxidation, and mineral dissolution of illite–smectite gave soluble cations like Ca^{2+}, Al^{3+}, Fe^{3+}, and Fe^{2+} as presented in Fig. 19a. The generated Fe^{2+} and Al^{3+} attack the bacteria via oxidation, destroying the multiple cellular components. Also, the hydrogen peroxide released through the cell envelops and reacts with the intercellular Fe^{2+} to form radicals that react or oxidize the protein and DNA molecules, thus activating the SOS stress response as shown in Fig. 19b.

Although a lot of findings on the antibacterial activity of clay have been documented, robust applications of clay-based nanocomposites such as clay/TiO_2, clay/ZnO, and clay/TiO_2/ZnO in microbial water treatment are not yet fully established. However, the information obtained so far signifies that these nanocomposites could emerge as a promising alternative for the removal of bacteria in water.

The mechanism of the antibacterial activity of clay-based nanocomposites can be classified into two stages namely: adhesion and killing. The application of nanoparticles and nanocomposites strongly depends on the classes or types of bacteria in water and the physicochemical characteristics of the nanomaterials. Other parameters worthy of consideration are involved in particle size concentration, morphology, pH, and calcination temperature of the nanomaterials.

The antibacterial study on ZnO–nanoclay hybrids against *Escherichia coli* and *Staphylococcus aureus* was conducted under the influence of contact time and temperature by Garshasbi et al. (2017). The nanocomposites were characterized by XRD, XRF, SEM, and UV–Vis diffuse reflectance spectroscopy. It was established that the two aforementioned factors affected the pore sizes of the nanoclay particles and the type of bacteria in the results. The obtained results indicated that the toxic effect on the bacteria was attributable to the photocatalytic activity of ZnO nanoparticles, along with the generation of hydrogen peroxide leading to the degradation of the cell wall of the bacteria.

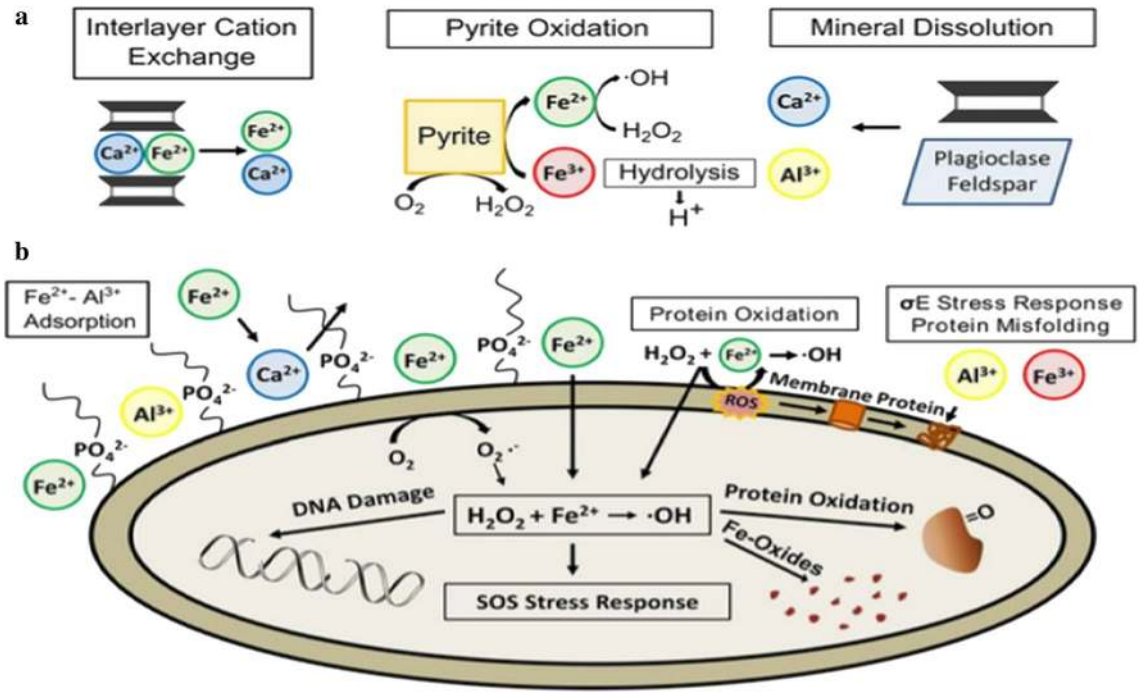

Fig. 19 The mechanism of antimicrobial activity of Oregon Blue clays

In the study of Copcia et al. (2013), ZnO/clinoptilolite and $ZnTiO_3$/clinoptilolite nanoparticles were used against Gram-negative *E. coli* and Gram-positive *S. aureus*. The composites were characterized using XRD, SEM, and EDX. Their results showed that ZnO/clinoptilolite improved the antimicrobial effect against *S. aureus*, while TiO/$ZnTiO_3$/clinoptilolite had a higher better antimicrobial effect on *E. coli*. More so, in the work of Mariselvi and Alagumuthu (2016), TiO_2/illite nanocomposites were synthesized and characterized using XRD, SEM, TEM, and UV–Vis spectroscopy. The antibacterial activity of the as-obtained nanocomposites against *E. coli*, *S. aureus,* and Bacillus were determined. It was established that the as-synthesized nanocomposites showed promising antibacterial activities against the selected bacterial species. The performance of as-synthesized zinc/bentonite clay as an antibacterial material was studied by Pouraboulghasem et al. (2016). The produced nanocomposites showed promising antibacterial features against *E. coli*.

Silver–zinc oxide nanoparticles were immobilized on the surface of bentonite and characterized using XRD, TEM, FTIR, and BET by Motshekga et al. (2013). They reported that the antibacterial activities of the nanocomposites were pretty good. In other report by Motshekga et al. (2015, 2016), blends of silver–zinc oxide bentonite chitosan nanocomposites and three composites (Ag/bentonite/chitosan, ZnO/bentonite/chitosan and silver/ZnO/bentonite/chitosan nanocomposites were evaluated for their antimicrobial activities against gram-negative *E. coli* and gram-positive Enterococcus faecalis bacteria, respectively. It was concluded that silver/ZnO/bentonite/chitosan nanocomposites proved to be the best bactericide.

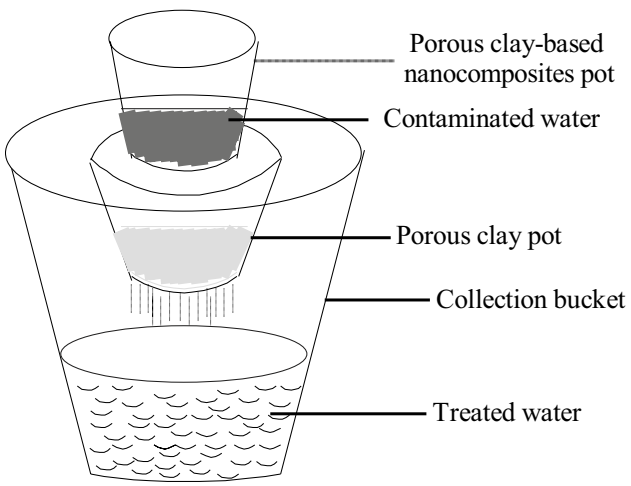

Fig. 20 The mini-scale nanocomposite filtration technique

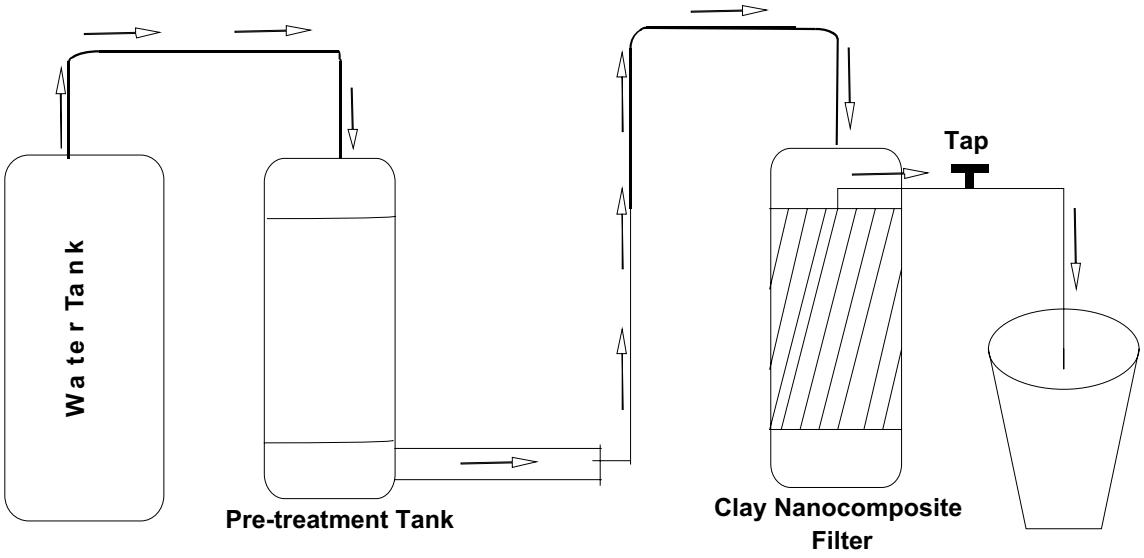

Fig. 21 The large-scale nanocomposite filtration technique

The need for stringent applications of nanoparticles and nanocomposites in water treatment

As earlier mentioned, nanomaterials have drawbacks in their applications. One of the principal difficulties of the two nanoparticles under consideration, TiO_2 and ZnO, is the large bandgap energy of the photocatalysts which require excitation by UV on applications during photodegradation of the contaminants in wastewater. In most articles, these nanoparticles are not classified as pollutants but their stability in water is paramount in assessing their potential risks. Considering their application in water, another crucial problem is regeneration. These nanoparticles in suspension are difficult to recover, and therefore, effort needs to be devoted in order to overcome these problems. To achieve this, incorporating nanoparticles in clay has attracted much attention. Thus, filtration techniques may become paramount for the removal of pollutants in wastewater. This technology can be improved through the production of nano-based filters. This nano-based filtration technology as shown in Figs. 20 and 21 will allow for regeneration and reducing toxicity and cost, thus giving room for industrial-scale production.

On the other hand, clay has proved to be a promising natural material for removing pollutant and microorganism from water due to its physicochemical characteristics, but the use of clay nanocomposites as filters for wastewater treatment is still lacking. This review gives insight into the importance and literature on different of clays, clay/TiO_2, and clay/ZnO blends for adsorption studies, but integrated method like adsorption and filtration technique for wastewater treatment is still lacking. More so, there is little or no information available in previous research on the fabrication of nanofilters from the combination of kaolin with TiO_2 and ZnO nanoparticles (nanocomposites) for the removal of pollutants from wastewater. In order to materialize this goal, research needs to focus on developing nano-based filters which will require less energy, less intensive synthesis techniques, and cheap feedstock. This can be accomplished by examining the compositions of clay minerals and their mechanical properties before employing them for applications.

Conclusion

This review paper offers an insight into recent developments in the field of clay nanocomposites used for wastewater treatment. Insight into the use of clay minerals, preparation, and characterization of TiO_2 and ZnO nanoparticles and their application as composites in water treatment has been reviewed. Nanotechnological applications of nanoclay materials, TiO_2, ZnO, and their composites are capable of adsorbing, photocatalyzing, and biological elimination of pollutants in wastewater. The challenges such as the recovery and reuse of the nanomaterial and nanocomposites need to be overcome in order to effectively apply this technology. However, the removal of foul-smelling pollutants in wastewater can be achieved through water filtration nanotechnology. The production of nano-based filters through the combination of clay/TiO_2/ZnO nanocomposites should be put into practice in innovative water treatment processes. Thus, integration techniques during water treatment incorporate adsorption, photocatalysis, and biological treatments are recommended to ensure sufficient quality of water.

Acknowledgements The authors appreciate the financial support received from the Tertiary Education Trust Fund (TETFund) of Nigeria under a Grant Number TETFUND/FUTMINNA/2017/01.

Compliance with ethical standards

Conflict of interest The authors declared that they have no conflict of interest.

References

Abdullah AK, Awad S, Zaraket J, Salame C (2017a) Synthesis of ZnO Nanopowders by using Sol-gel and studying their structural and electrical properties at different temperature. Energy Procedia 119:565–570

Abdullah NSA, So'aib S, Krishnan J (2017b) Effect of calcination temperature on ZnO/TiO_2 composite in photocatalytic treatment of phenol under visible light. Malays J Anal Sci 21(1):173–181

Acosta-Humánez M, Montes-Vides L, Almanza-Montero O (2015) Sol–gel synthesis of zinc oxide nanoparticle at three different temperatures and its characterization via XRD, IR and EPR. DYNA 83(195):224–228

Adeyemo AA, Adeoye IO, Bello OS (2015) Adsorption of dyes using different types of clay: a review. Appl Water Sci 7(2):543–568

Agarthan L, Kapusuz D, Park J, Ozturk A (2013) Effect of H_2O/TEOT ratio on photocatalytic activity of sol-gel derived TiO_2 powder. Nanomater Energy 2:280–287

Aguiar JE, Cecilia JA, Tavares PAS, Azevedo DCS, Castellón ER, Lucena SMP, Silva-Junior IJ (2017) Adsorption study of reactive dyes onto porous clay heterostructures. Appl Clay Sci 135:36–44

Akhter M, Habib G, Qama SU (2018) Application of electrodialysis in waste water treatment and impact of fouling on process performance. J Membr Sci Technol 8(2):1–8

Akkari M, Aranda P, Ben Rhaiem H, Amara AB, Ruiz-Hitzky E (2015) ZnO/clay nanoarchitectures: synthesis, characterization and evaluation as photocatalysts. Appl Clay Sci 131:131–139

Akkari M, Aranda P, Mayoral A, García-Hernández M, Amara ABH, Ruiz-Hitzky E (2017) Sepiolite nanoplatform for the simultaneous assembly of magnetite and zinc oxide nanoparticles as photocatalyst for improving removal of organic pollutants. J Hazard Mater 340:281–290

Akkari M, Aranda P, Belver C, Bediac J, Amara AB, Ruiz-Hitzky E (2018) ZnO/sepiolite heterostructured materials for solar photocatalytic degradation of pharmaceuticals in wastewater. Appl Clay Sci 156:104–109

Al-Essa K, Khalili F (2018) Heavy metals adsorption from aqueous solutions onto unmodified and modified jordanian kaolinite clay: batch and column techniques. Am J Appl Chem 6(1):25–34

Al-Hamadani YAJ, Chu KH, Son A, Heo J, Her N, Jang M, Park CM, Yoon Y (2015) Stabilization and dispersion of carbon nanomaterials in aqueous solutions: a review. Sep Purif Technol 156:861–874

Aljlil SA, Alsewailem FD (2014) Adsorption of Cu & Ni on bentonite clay from waste water. Athens J Nat Form Sci 1(1):21–30

Alshameri A, He H, Zhu J, Xi Y, Zhu R, Ma L, Tao Q (2018) Adsorption of ammonium by different natural clay minerals: characterization, kinetics and adsorption isotherms. App Clay Sci 159:83–93

Alwan RM, Kadhim QA, Sahan KM, Ali RA, Mahdi RJ, Kassim NA, Jassim AN (2015) Synthesis of zinc oxide nanoparticles via sol–gel route and their characterization. Nanosci Nanotechnol 5(1):1–6

Amin MT, Alazb AA, Shafiq M (2015) Adsorptive removal of reactive black 5 from wastewater using bentonite clay: isotherms, kinetics and thermodynamics. Sustainability 7:15302–15318

Anirudhan TS, Ramachandran M (2015) Adsorptive removal of basic dyes from aqueous solutions by surfactant modified bentonite clay (organoclay): kinetic and competitive adsorption isotherm. Proc Saf Environ Prot 95:215–225

Annan E, Agyei-Tuffour B, Bensah YD, Konadu DS, Yaya A, Onwona-Agyeman B, Nyankson E (2018) Application of clay ceramics and nanotechnology in water treatment: a review. Cogent Eng 5(1):1–35

Ansari MM, Arshad M, Tripathi P (2015) Study of ZnO and Mg-doped ZnO nanoparticles by sol–gel process. AIP Conf Proc 1665:050123-1–050123-3

Aryanto D, Jannah WN, Sudiro MT, Wismogroho AS, Sebayang P, Sugianto A, Marwoton P (2017) Preparation and structural characterization of ZnO thin films by sol–gel method. IOP Conf Ser J Phys Conf Ser 817:1–8

Ashraf R, Riaz S, Hhaleeq-ur-Rehman M, Naseem S (2013) Synthesis and characterization of ZnO nanoparticles. Adv Nano, Biomech Robot Energy Res (ANBRE) 13:287–296

Assi N, Azar PA, Tehrani MS, Husain SW, Darwish M, Pourmand S (2017) Synthesis of ZnO-nanoparticles by microwave-assisted sol–gel method and its role in photocatalytic degradation of food dye Tartrazine (Acid Yellow 23). Int J Nano Dimens 8(3):241–249

Avrami M (1940) Kinetics of phase change: transformation-time relations for random distribution of nuclei. J Chem Phys 8:212–224

Ba-Abbad MM, Kadhum AAH, Mohamad AB, Takriff MS, Sopian K (2013a) The effect of process parameters on the size of ZnO nanoparticles synthesized via the sol–gel technique. J Alloys Compd 550:63–70

Ba-Abbad MM, Kadhum AAH, Mohamad AB, Takriff MS, Sopian K (2013b) Optimization of process parameters using D-optimal design for synthesis of ZnO nanoparticles via sol–gel technique. J Indus Eng Chem 19(1):99–105

Ba-Abbad MM, Takriff MS, Benamor AB, Nasser MS, Mahmoudi E, Mohammad AW (2017) Synthesis and characterization of Sm^{3+}-doped ZnO nanoparticles via a sol–gel method and their photocatalytic application. J Sol Gel Sci Technol 85(1):178–190

Bagheri S, Chekin F, Abd-Hamid SB (2014) Gel-assisted synthesis of anatase TiO_2 nanoparticles and application for electrochemical determination of L-tryptophan. Russ J Electrochem 50(10):947–952

Bahar M, Mozaffari M, Esmaeili S (2017) Effect of different alcohols, gelatinizing times, calcination and microwave on characteristics of TiO_2 nanoparticles synthesized by sol–gel method. J Theor Appl Phys 11:79–86

Bel-Hadjltaief H, Galvez ME, Zina MB, Da Costa P (2014) TiO_2/clay as a heterogeneous catalyst in photocatalytic/photochemical

oxidation of anionic reactive blue 19. Arab J Chem 12:1454–1462 **(in Press)**

Bel-Hadjltaief H, Ben Zina M, Galvez ME, Da Costa P (2016) Photocatalytic degradation of methyl green dye in aqueous solution over natural clay-supported ZnO–TiO_2 catalysts. J Photochem Photobiol A Chem 315:25–33

Bel-Hadjltaief H, Ben Ameur S, Da Costa P, Ben Zina M, Galvez ME (2018) Photocatalytic decolourization of cationic and anionic dyes over ZnO nanoparticle immobilized on natural Tunisian clay. Appl Clay Sci 152:148–157

Belver C, Han C, Rodriguez JJ, Dionysiou DD (2016) Innovative W-doped titanium dioxide anchored on clay for photocatalytic removal of atrazine. Catal Today 280:21–28

Bhardwaj R, Bharti A, Singh JP, Chae KH, Goyal N, Gautam S (2018) Structural and electronic investigation of ZnO nanostructures synthesized under different environments. Heliyon 4:1–21

Bhattachajee C, Samanta HS, Das R (2016) Influence of nanoparticles for wastewater treatment—a short review. Austin Chem Eng 3(3):1036–1041

Boutra B, Trari M (2018) Solar photodegradation of a textile azo dye using synthesized ZnO/Bentonite. Water Sci Technol 75(5):1211–1220

Boyd GE, Adamson AW, Myers LS (1947) The exchange adsorption of ions from aqueous solutions by organic zeolites. II. Kinetics. J Am Chem Soc 69:2836–2848

Brigatti MF, Galan E, Theng BKG (2013) Structure and mineralogy of clay minerals. In: Bergaya F, Lagaly G (eds) Handbook of clay science, part A, 2nd edn. Elsevier, Amsterdam, pp 21–82

Brintha SR, Ajitha M (2015) Synthesis and characterization of ZnO nanoparticles via aqueous solution, sol–gel and hydrothermal methods. IOSR J Appl Chem (IOSR-JAC) 8(11):66–72

Bruanuer S, Emmett PH, Teller E (1938) Adsorption of gases in multimolecular layers. J Am Chem Soc 60:309–316

Caponi N, Collazzo GC, Jahn SL, Dotto GL, Mazutti MA, Foletto EL (2017) Use of Brazilian kaolin as a potential low-cost adsorbent for the removal of malachite green from colored effluents. Mater Res 1:1–9

Cardenas MAR, Ali I, Lai FY, Dawes L, Thier R, Rajapakse J (2016) Removal of micropollutants through a biological wastewater treatment plant in a subtropical climate, Queensland-Australia. J Environ Health Sci Eng 14(14):1–10

Carrier B, Wang L, Vandamme M, Pellenq RJM, Bornert M, Tanguy A, Van Damme H (2013) ESEM study of the humidity-induced swelling of clay films. Langmuir 29:12823–12833

Carrier B, Vandamme M, Pellenq RJM, Van Damme H (2014) Elastic properties of swelling clay particles at finite temperature upon hydration. J Phys Sci 118:8933–8943

Cassaignon S, Koelsch M, Jolivet JP (2007) From $TiCl_3$ to TiO_2 nanoparticles (anatase, brookite and rutile): thermohydrolysis and oxidation in aqueous medium. J Phys Chem Solids 68:695–700

Chen D, Zhu H, Wang X (2014a) A facile method to synthesize the photocatalyticTiO_2/montmorillonite nanocomposites with enhanced photoactivity. Appl Surf Sci 19:158–166

Chen Y, Xu X, Fang J, Zhou G, Liu Z, Wu S, Xu W, Chu J, Zhu X (2014b) Synthesis of BiOI-TiO_2 composite nanoparticles by microemulsion method and study on their photocatalytic activities. Sci World J 1:1–8

Chinoune K, Bentaleb K, Bouberka Z, Nadim A, Maschke U (2016) Adsorption of reactive dyes from aqueous solution by dirty bentonite. Appl Clay Sci 123:64–75

Chouchene B, Chaabane TB, Mozet K, Girot E, Corbel S, Balan L, Medjandi G, Schneider R (2017) Porous Al-doped ZnO rods with selective adsorption properties. Appl Surf Sci 409:102–110

Chung YT, Ba-Abbad MM, Mohammad AW, Hairom NHH, Benamor A (2015) Synthesis of minimal-size ZnO nanoparticles through sol–gel method: taguchi design optimisation. Mater Des 87:780–787

Copcia VE, Hristodor CM, Dunca S, Iordanova R, Cheva AB, Forna NC, Sandu I (2013) Synthesis and antibacterial properties of ZnO/clinoptilolite and TiO_2/$ZnTiO_3$/clinoptilolite powders. Rev Chim (Bucharest) 64(9):978–981

da Silva Lopes J, Rodrigues WV, Oliveira VV, Braga ADNS, da Silva RT, França AAC, da Paz EC, Osajima JA, da Silva Filho EC (2019) Modification of kaolinite from Pará/Brazil region applied in the anionic dye photocatalytic discoloration. Appl Clay Sci 168:295–303

Dale AL, Casman EA, Lowry GV, Lead JR, Viparelli E, Baalousha M (2015) Modeling nanomaterial environmental fate in aquatic systems. Environ Sci Technol 49(5):2587–2593

Dalvandi M, Ghasemi B (2013) Synthesis of titanium dioxide nanopowder via sol–gel method at ambient temperature. J Sol Gel Technol 6(1):68–72

Dariania RS, Esmaeilia A, Mortezaalia A, Dehghanpour S (2016) Photocatalytic reaction and degradation of methylene blue on TiO_2 nano-sized particles. Optik 127:714–7154

Davis D, Singh S (2016) ZnO nanoparticles synthesis by sol–gel method and characterization. Indian J Nanosci 4(1):1–4

De Boer JH (1953) The dynamical character of adsorption. Oxford University Press, Oxford

de Oliveira da Mota I, Adilson de Castro J, de Góes Casqueira R, de Oliveira Junior AG (2015) Study of electroflotation method for treatment of wastewater from washing soil contaminated by heavy metals. J Mater Res Technol 4(2):109–113

Dědková K, Janíková B, Matějová K, Peikertová P, Neuwirthová L, Holešinský J, Kukutschová J (2015) Preparation, characterization and antibacterial properties of ZnO/kaoline nanocomposites. J Photochem Photobiol B Biol 135:17–22

de-Luna MDG, Laciste MT, Tolosa NC, Lu M (2018) Effect of catalyst calcination temperature in the visible light photocatalytic oxidation of gaseous formaldehyde by multi-element doped titanium dioxide. Environ Sci Pollut Res 25:15216–15225

Devi M, Panigrahi MR, Singh UP (2014) Synthesis of TiO_2 nanocrystalline powder prepared by a sol–gel technique using TiO_2 powder reagent. Adv Appl Sci Res 5(3):140–145

Díaz-de-León CL, Olivas-Armendariz I, Hernández-Paz JF, Gómez-Esparza CD, Reyes-Blas H, Hernández-González M, Velasco-Santos C, Rivera-Armenta JL, Rodríguez-González CA (2017) Synthesis by sol–gel and cytotoxicity of zinc oxide nanoparticles using wasted alkaline batteries. Dig J Nanomater Biostruct 12(2):371–379

Divya C, Janarthanan B, Premkumar S, Chandrasekaran J (2017) Titanium dioxide nanoparticles preparation for dye-sensitized solar cells applications using sol–gel method. J Adv Phys Sci 1(1):4–6

Djellabi R, Ghorab MF, Cerrato G, Morandi S, Gatto S, Oldani V, Di Michele A, Bianchi CL (2014) Photoactive TiO_2–montmorillonite composite for degradation of organic dyes in water. J Photochem Photobiol A Chem 295:57–63

Dodoo-Arhin D, Buabeng FP, Mwabora JM, Amaniampong PN, Agbe H, Nyankson E, Obada DO, Asiedu NY (2018) The effect of titanium dioxide synthesis technique and its photocatalytic degradation of organic dye pollutants. Heliyon 4(7):1–23

Dubinin MM, Radushkevich LV (1947) Equation of the characteristic curve of activated charcoal. Proc Acad Sci Phys Chem Sect 55:331–333

Elbushra H, Ahmed M, Wardi H, Eassa N (2018) Synthesis and characterization of TiO_2 using the sol–gel method at different annealing temperatures. Mater Res Soc 230:1–9

El-Ghoul J, Kraini M, El-Mir L (2015) Synthesis of Co-doped ZnO nanoparticles by sol-gel method and its characterization. J Mater Sci: Mater Electron 26(4):2555–2562

EL-Mekkawi DM, Labib AA, Mousa HA, Galal HR, Mohamed WAA (2017) Preparation and characterization of nano titanium dioxide photocatalysts via sol–gel method over narrow ranges of varying parameters. Oriental J Chem 33(1):41–51

Elovich SY, Larinov OG (1962) Theory of adsorption from solutions of non-electrolytes on solid(I) equation adsorption from solutions and the analysis of its simplest form, (II) verification of the equation of adsorption isotherm from solutions. Izv Akad Nauk SSSR Otd Khimicheskikh Nauk 2(2):209

Fajriati I, Mudasir A, Wahyuni ET (2017) The Effect of pH and aging time on the synthesis of TiO_2-chitosan nanocomposites as photocatalyst by sol–gel method at room temperature. Molekul 12(2):117–125

Fernández-Catalá J, Cano-Casanova L, Lillo-Ródenas MA, Berenguer-Murcia A, Cazorla-Amorós D (2017) Synthesis of TiO_2 with hierarchical porosity for the photooxidation of propene. Molecules 22:2243–2259

Flory PJ (1941) Thermodynamics of high polymer solutions. J Chem Phys 9:660

Freundlich HMF (1906) Over the adsorption in solution. J Phys Chem 57:385–470

Fu R, Yin Q, Guo X, Tong X, Wang X (2017) Evolution of mesoporous TiO_2 during fast sol–gel synthesis. Res Chem Intermed 43(11):6433–6445

Garshasbi N, Ghorbanpour M, Nouri A, Lotfiman S (2017) Preparation of zinc oxide-nanoclay hybrids by alkaline ion exchange method. Braz J Chem Eng 34(4):1055–1063

Gehrke I, Geiser A, Somborn-Schulz A (2015) Innovations in nanotechnology for water treatment. Nanotechol Sci Appl 8:1–17

Golsheikh AM, Kamali KZ, Huang NM, Zak AK (2017) Effect of calcination temperature on performance of ZnO nanoparticles for dye-sensitized solar cells. Powder Technol 329:282–287

Gómez-de-Salazar JM, Duduman CM, Gonzalez MJ, Palamarciuc I, Pérez MIB, Carcea I (2016) Research of obtaining TiO_2 by sol–gel method using titanium isopropoxide TIP and tetra-n-butyl orthotitanate TNB. IOP Conf Ser Mater Sci Eng 145:1–6

González P, Pliego-Cuervo YB (2014) Adsorption of Cd(II), Hg(II) and Zn(II) from aqueous solution using mesoporous activated carbon produced from Bambusa vulgaris striata. Chem Eng Res Des 92(11):2715–2724

Govindaraj R, Pandian MS, Ramasamy P, Mukhopadhyay S (2015) Sol–gel synthesized mesoporous anatase titanium dioxide nanoparticles for dye-sensitized solar cell (DSSC) applications. Bull Mater Sci 38(2):291–296

Guillaume PLA, Chelaru AM, Visa M, Lassiné O (2018) "Titanium oxide-clay" as adsorbent and photocatalysts for wastewater treatment. J Membr Sci Technol 8(1):176–186

Habibi MH, Karimi B (2014) Preparation, characterization, and application of zinc oxide nanoparticles by sol–gel pyrolysis method: influence of annealing temperature on crystalline phases. Synth React Inorg Metal Org Nano Metal Chem 44(9):1291–1298

Hadjltaief HB, Zina MB, Galvez ME, Costa PD (2017) Photocatalytic degradation of methyl green dye in aqueous solution over natural clay-supported ZnO–TiO_2 catalysts. J Photochem Photobiol A Chem 315:25–33

Haider A, Jameel ZN, Taha SY (2015) Synthesis and characterization of TiO_2 nanoparticles via sol–gel method by pulse laser ablation. Eng Technol J 33(5):761–771

Haider AJ, Al-Anbari RH, Kadhim GR, Salame CT (2017) Exploring potential environmental application TiO_2 nanoparticles. Energy Procedia 119:332–345

Hajjaji W, Andrejkovičová S, Pullar RC, Tobaldi DM, Lopez-galindo A, Jammousi F, Rocha F, Labrincha JA (2016) Effective removal of anionic and cationic dyes by kaolinite and TiO_2/kaolinite composites. Clay Miner 51:19–27

Haq S, Rehman W, Waseem M, Javed R, Rehman M, Shahid M (2018) Effect of heating on the structural and optical properties of TiO_2 nanoparticles: antibacterial activity. Appl Nanosci 8:11–18

Harun K, Mansor N, Ahmad ZA, Mohamad AZ (2016) Electronic properties of ZnO nanoparticles synthesized by sol–gel method: a LDA + U calculation and experimental study. Procedia Chem 19:125–132

Hayle ST, Gonfa GG (2014) Synthesis and characterization of titanium oxide nanomaterials using sol–gel method. Am J Nanosci Nanotechnol 2(1):1–7

He F, Ma F, Li J, Li T, Li G (2014) Effect of calcination temperature on the structural properties and photocatalytic activities of solvothermal synthesized TiO_2 hollow nanoparticles. Ceram Int 40:6441–6446

Hedayati K (2015) Fabrication and optical characterization of zinc oxide nanoparticles prepared via a simple sol–gel method. J Nanostruct (JNS) 5(4):395–401

Huang X, Qu Y, Cid CA, Finke C, Hoffmann MR, Lim K, Jiang SC (2016) Electrochemical disinfection of toilet wastewater using wastewater electrolysis cell. Water Res 92:164–172

Huang Z, Li Y, Chen W, Shi J, Zhang N, Wang X, Li Z, Gao L, Zhang Y (2017) Modified bentonite adsorption of organic pollutants of dye wastewater. Mater Chem Phys 202:266–276

Huanhuan W, Peijiang Z, Jia W, Yifei W, Junchong W, Hongju Z, Rui G, Yali Z (2018) Synthesis and characterization of rectorite/ZnO/TiO_2 composites and their properties of adsorption and photocatalysis for the removal of methylene blue dye. J Wuhan Univ Technol 33(3):729–734

Ibrahim MM, Asal S (2017) Physicochemical and photocatalytic studies of Ln^{3+}- ZnO for water disinfection and wastewater treatment applications. J Molecular Structure 1149:404–413

Ibrahim SA, Sreekantan S (2010) Effect of pH on TiO_2 nanoparticles via sol gel method. In: International conference on X-rays and related techniques in research and industry, June 9–10, 2010, Aseania Resort Langkawi, Malaysia, pp 84–87

Islam M, Basu S (2015) Effect of morphology and pH on (photo) electrochemical degradation of methyl orange using TiO_2/Ti mesh photocathode under visible light. J Environ Chem Eng 3:2323–2330

Islam SZ, Nagpure S, Kim DY, Rankin SE (2017) Synthesis and catalytic applications of non-metal doped mesoporous titania. Inorganics 5(15):1–43

Jeevanandam J, Barhoum A, Chan YS, Dufresne A, Danquah MK (2018) Review on nanoparticles and nanostructured materials: history, sources, toxicity and regulations. Beilstein J Nanotechnol 9:1050–1074

Ji Z (2018) Treatment of heavy-metal wastewater by vacuum membrane distillation: effect of wastewater properties. IOP Conf Ser Earth Environ Sci 108:1–4

Jin J, Hao A, Wang G, He X, Zhang W, Chen Q (2014) The study of different pH values on the morphology of ZnO nanoparticles via sol–gel technology. J Chem Pharm Res 6(6):1676–1680

Jossens L, Prausnitz JM, Fritz W, Schlunder EU, Myers AL (1978) Thermodynamics of multi-solute adsorption from dilute aqueous solutions. Chem Eng Sci 33(8):1097–1106

Jovanovic DS (1969) Physical adsorption of gases I: isotherms for monolayer and multilayer adsorption. Colloid Polym Sci 235:1203–1214

Jurablu S, Farahmandjou M, Firoozabadi TP (2015) Sol–gel synthesis of zinc oxide (ZnO) nanoparticles: study of structural and optical properties. J Sci Islamic Rep Iran 26(3):281–285

Kadhim WA, Bin-Ab-Rahim MH (2017) Surfactant-less sol–gel technique for the synthesis of Mg-ZnO nanoparticle. Fluid ChE MATEC Web Conf 111:1–4

Kaler V, Duchaniya RK, Pandel U (2016) Synthesis of nano-titanium dioxide by sol–gel route. In: 2nd international conference on

emerging technologies: micro to nano 2015 (ETMN-2015). AIP conference proceeding, vol 1724, pp 020127-1–020127-4
Kaneva N, Bojinova A, Papazova K (2016) Photocatalytic degradation of reactive black 5 and malachite green with ZnO and lanthanum doped nanoparticles. J Phys: Conf Ser 682:1–7
Kassahun SK, Kiflie Z, Shin DW, Park SS, Jung WY, Chung YR (2017) Optimization of sol-gel synthesis parameters in the preparation of N-doped TiO_2 using surface response methodology. J Sol Gel Sci Technol 82(2):322–334
Kavitha M, Gopinathan C, Pandi P (2014) Synthesis and characterization of TiO_2 nanopowders in hydrothermal and sol–gel method. Int J Adv Res Technol 2(4):102–108
Kayani ZN, Saleemi F, Batool I (2015) Effect of calcination temperature on the properties of ZnO nanoparticles. Appl Phys A Mater Sci Process 1:1–8
Khade GV, Suwarnkar MB, Gavade NL, Garadkar KM (2016) Sol-gel microwave-assisted synthesis of Sm-doped TiO_2 nanoparticles and their photocatalytic activity for the degradation of methyl orange under sunlight. J Mater Sci: Mater Electron 27:6425–6432
Khan H (2017) Sol-gel synthesis of TiO_2 from $TiOSO_4$: characterization and UV photocatalytic activity for the degradation of 4-chlorophenol. React Kinet Mechan Catal 121(2):811–832
Khan W, Khan ZA, Saad AA, Shervani S, Saleem A, Naqvi AH (2013) Synthesis and characterization of Al doped ZnO nanoparticles. Int J Mod Phys Conf Ser 22:630–636
Khan MF, Ansari AH, Hameedullah M, Ahmad E, Husain FM, Zia Q, Baig U, Zaheer MR, Alam MM, Khan AM, AlOthman ZA, Ahmad I, Ashraf GM, Aliev G (2016) Sol–gel synthesis of thorn-like ZnO nanoparticles endorsing mechanical stirring effect and their antimicrobial activities: potential role as nano-antibiotics. Sci Rep 6:1–12
Khan I, Saeed K, Khan I (2017) Nanoparticles: properties, applications and toxicities. Arab J Chem 12:908–931 **(in Press)**
Kiseler AVC (1958) Vapour adsorption in the formation of adsorbate molecule complexes on the surface. Kolloid Zhur 20:338–348
Koble RA, Corrigan TE (1952) Adsorption isotherms for pure hydrocarbons. Ind Eng Chem 44(2):383–387
Konduri MKR, Fatehi P (2017) Influence of pH and ionic strength on flocculation of clay suspensions with cationic xylan copolymer. Colloids Surf A 530:20–32
Kumar A, Yadav N, Bhatt M, Mishra NK, Chaudhary P, Singh R (2015) Sol–gel derived nanomaterials and its applications: a review. Res J Chem Sci 5(12):98–105
Lagergren S (1898) About the theory of so-called adsorption of soluble substances. K Sven Vetensk 4:1–39
Langmuir I (1916) The constitutional and fundamental properties of solids and liquids. J Am Chem Soc 38:2221–2295
Laysandra L, Sari MWMK, Soetaredjo FE, Foe K, Putro JN, Kurniawan A, Ju Y, Ismadji S (2017) Adsorption and photocatalytic performance of bentonite-titanium dioxide composites for methylene blue and rhodamine B decoloration. Heliyon 3:1–22
Lei C, Pi M, Jiang C, Cheng B, Yu J (2017) Synthesis of hierarchical porous zinc oxide (ZnO) microspheres with highly efficient adsorption of Congo red. J Colloid Interface Sci 490:242–251
Li H, Wang H, Liu Q, Tan Y, Jiang N, Lin Y (2016) Evaporation process for treating high-salinity industrial wastewater at low temperatures and ambient pressure. Des Water Treat 1:1–13
Lin D, Zhou S, Lu L, Shi-yang C, Ling-fang Y, Xiu-zhen Y, Li-shan L (2014) Adsorption of hexavalent chromium onto kaolin clay-based adsorbent. J Cent South Univ 21:3918–3926
Lin JC, Sopajaree K, Jitjanesuwan T, Lu M (2018) Application of visible light on copper-doped titanium dioxide catalyzing degradation of chlorophenols. Sep Purif Technol 191:233–243
Livingston HK (1949) The cross-sectional areas of molecules L84 adsorbed on solid surfaces. J Colloid Sci 4:447–458
Liu Z, Wang R, Kan F, Jiang F (2014) Synthesis and characterization of TiO_2 nanoparticles. Asian J Chem 26(3):655–659
Liu R, Ji Z, Wang J, Zhang J (2018) Mesocrystalline TiO_2/sepiolite composites for the effective degradation of methyl orange and methylene blue. Front Mater Sci 12(3):292–303
Lofrano G, Carotenuto M, Libralato G, Domingos RF, Markus A, Dini L, Gautam RK, Baldantoni D, Rossi M, Sharma SK, Chattopadhyaya MC, Giugni M, Meric S (2016) Polymer functionalized nanocomposites for metals removal from water and wastewater: an overview. Water Res 92:22–37
Lu H, Wang J, Wang T, Wang N, Bao Y, Hao H (2017) Crystallization techniques in wastewater treatment: an overview of applications. Chemosphere 173:474–484
Lukman S, Essa MH, Mu'azu ND, Bukhari A, Basheer C (2013) Adsorption and desorption of heavy metals onto natural clay materials: influence of initial pH. J Environ Sci Technol 6(1):1–15
Mabroukia H, Akretchea DE (2015) Diclofenac potassium removal from water by adsorption on natural and pillared clay. Desalin Water Treat 57(13):6033–6043
Mahammedi F, Benguella B (2016) Adsorption of methylene blue from aqueous solutions using natural clay. J Mater Environ Sci 7(1):85–292
Mallika GN, Narsaiah TB (2017) Synthesis of TiO_2 nanoparticles using sol–gel method for the treatment of pharmaceutical wastewater. IJSRD Int J Sci Res Dev 5(6):498–501
Manikandan B, Endo T, Kaneko S, Murali KR, John R (2017) Properties of sol–gel synthesized ZnO nanoparticles. J Mater Sci: Mater Electron 29(11):9474–9485
Marami MB, Farahmandjou M, Khoshnevisan B (2018) Sol–gel synthesis of Fe-doped TiO_2 nanocrystals. J Electron Mater 47(7):3741–3748
Mariselvi P, Alagumuthu G (2016) Synthesis, characterization and antibacterial activity of illite/TiO_2 nanocomposites. Int J Appl Res 2(4):553–556
Martins AC, Cazetta AL, Pezoti O, Souza JRB, Zhang T, Pilau EJ, Asefa T, Almeida VC (2017) Sol–gel synthesis of new TiO_2/activated carbon photocatalyst and its application for degradation of tetracycline. Ceram Int 43(5):4411–4418
Mathews NR, Cortes Jacome MA, Angeles-Chavez C, Toledo Antonio JA (2014) Fe doped TiO_2 powder synthesized by sol–gel method: structural and photocatalytic characterization. J Mater Sci: Mater Electron 26(8):5574–5584
Mishra A, Mehta A, Sharma M, Basu S (2017) Enhanced heterogeneous photodegradation of VOC and dye using microwave synthesized TiO_2/Clay nanocomposites: a comparison study of different type of clays. J Alloys Compds 694:574–580
Modwi A, Abbo MA, Hassan EA, Houas A (2016) Effect of annealing on physicochemical and photocatalytic activity of Cu5% loading on ZnO synthesized by sol–gel method. Mater Electron, J Mater Sci, pp 1–11
Mohan AC, Renjanadevi B (2016) Preparation of zinc oxide nanoparticles and its characterization using scanning electron microscopy (SEM) and x-ray diffraction (XRD). Procedia Technol 24:761–766
Mohite VS, Mahadik MA, Kumbhar SS, Kothavale VP, Moholkar AV, Rajpure KY, Bhosale CH (2015) Photo-electrocatalytic degradation of benzoic acid using sprayed TiO_2 thin films. Ceramic Int 41:2202–2208
Mohsenipour M, Shahid S, Ebrahimi K (2015) Nitrate adsorption on clay kaolin: batch tests. J Chem 1:1–7
Morales J, Maldonado A, de la M, Olvera L (2013) Synthesis and characterization of nanostructured TiO_2 anatase-phase powders obtained by the homogeneous precipitation method. In: 10th international conference on electrical engineering, computing

science and automatic control (CCE) Mexico City, Mexico. September 30–October 4, 2013
Morrison KD, Misra R, Williams LB (2016) Unearthing the antibacterial mechanism of medicinal clay: a geochemical approach to combating antibiotic resistance. Sci Rep 6:1–13
Motshekga SC, Ray SS, Onyango MS, Momba MNB (2013) Microwave-assisted synthesis, characterization and antibacterial activity of Ag/ZnO nanoparticles supported bentonite clay. J Hazard Mater 262:439–446
Motshekga SC, Ray SS, Onyango MS, Momba MNB (2015) Preparation and antibacterial activity of chitosan-based nanocomposites containing bentonite-supported silver and zinc oxide nanoparticles for water disinfection. Appl Clay Sci 114:330–339
Motshekga SC, Ray SS, Onyango MS, Momba MNB (2016) Development of silver and zinc oxide decorated nanoclay containing polymeric composites for water disinfection applications. AIP Conf Proc 1664:1–5
Mousa KM, Hadi HJ (2016) Coagulation/flocculation process for produced water treatment. Int J Curr Eng Technol 6(2):551–555
Mousavi S, Shahraki F, Aliabadi M, Haji A, Deuber F, Adlhart C (2019) Surface enriched nanofiber mats for efficient adsorption of Cr(VI) inspired by nature. J Environ Chem Eng 7(1):102817
Moussaoui R, Elghniji K, Mosbah MB, Elaloui E, Moussaoui Y (2017) Sol–gel synthesis of highly TiO_2 aerogel photocatalyst via high-temperature supercritical drying. J Saudi Chem Soc 21:751–760 **(in Press)**
Mukherjee S (2013) The science of clays: applications in industry, engineering, and environment. Springer, Heidelberg
Mutuma BK, Shao GN, Kim WD, Kim HT (2015) Sol–gel synthesis of mesoporous anatase-brookite and anatase-brookite-rutile TiO_2 nanoparticles and their photocatalytic properties. J Colloid Interface Sci 442:1–7
Nachit W, Touhtouh S, Ramzi Z, Zbair M, Eddiai A, Rguiti M, Bouchikhi A, Hajjaji A, Benkhouja K (2016) Synthesis of nanosized TiO_2 powder by sol–gel method at low temperature. Mol Cryst Liq Cryst 627:170–175
Nasirian M, Mehrvar M (2016) Modification of TiO_2 to enhance photocatalytic degradation of organics in aqueous solutions. J Environ Chem Eng 4:4072–4082
Oganisian K, Hreniak A, Sikora A, Gaworska-Koniarek D, Iwan A (2015) Synthesis of iron-doped titanium dioxide by sol–gel method for magnetic applications. Process Appl Ceram 9(1):43–51
Pavel K, Radovan K (2015) The effect of calcination on the structure of inorganic TiO_2 nanofibers. Oct 14th–16th 2015, Brno, Czech Republic, EU. NanoCon
Peeters B (2015) Wastewater sludge centrifugation before drying Chemical engineering, vol 122(4). Mcgraw Hill Incorporated Then Chemical Week Publishing Llc, New York, pp 56–60
Phonkhokkong T, Thongtem S, Thongtem CS, Phuruangrat A, Promnopas W (2016) Synthesis and characterization of TiO_2 nanopowders for fabrication of dye-sensitized solar cells. Dig J Nanomater Biostruct 11(1):81–90
Pinto ACS, Grossi L, Carvalho de Melo RA, Macedo de Assis T, Ribeiro VM, Amaral MSC, Figueiredo KC (2017) Carwash wastewater treatment by micro and ultrafiltration membranes: effects of geometry, pore size, pressure difference and feed flow rate in transport properties. J Water Proc Eng 17:143–148
Pookmanee P, Phanichphant S (2014) Titanium dioxide powder prepared by a sol–gel method. J Ceram Proc Res 10(2):167–170
Pouraboulghasem H, Ghorbanpour M, Shayegh M, Lotfiman S (2016) Synthesis, characterization and antimicrobial activity of alkaline ion-exchanged ZnO/bentonite nanocomposites. J Cent South Univ 23:787–792
Preethi S, Anitha A, Arulmozhi M (2016) A comparative analysis of the properties of zinc oxide (ZnO) nanoparticles synthesized by hydrothermal and sol–gel methods. Indian J Sci Technol 9(40):1–6
Preethi J, Farzana MH, Meenakshi S (2017) Photo-reduction of Cr(VI) using chitosan supported zinc oxide materials. Int J Biol Macromol 104:1783–1793
Rafati L, Ehrampoush MH, Rafati AA, Mokhtari M, Mahvi AH (2019) Fixed bed adsorption column studies and models for removal of ibuprofen from aqueous solution by strong adsorbent nano-clay composite. J Environ Health Sci Eng, pp 1–13
Rafiq Z, Nazir R, Shahwar D, Shah MR, Ali S (2014) Utilization of magnesium and zinc oxide nano-adsorbents as potential materials for treatment of copper electroplating industry wastewater. J Environ Chem Eng 2:642–651
Rahman A, Kishimoto N, Urabe T (2015) Adsorption characteristics of clay adsorbents-sepiolite, kaolin and synthetic talc-for removal of reactive yellow 138:1. Water Environ J 29:375–382
Rao BG, Mukherjee D, Reddy BM (2017) Novel approaches for preparation of nanoparticles. In: Ficai D, Grumezescu AM (eds) Nanostructures for novel therapy: synthesis, characterization and applications. Elsevier, London, UK, pp 1–36
Redlich O, Peterson DL (1959) A useful adsorption isotherm. J Phys Chem 63(6):1024
Rida K, Bouraoui S, Hadnine S (2013) Adsorption of methylene blue from aqueous solution by kaolin and zeolite. Appl Clay Sci 83–84:99–105
Roginsky SZ, Zeldovich YaB (1934) Acta Phys Chem USSR 1:554
Romeiro A, Freitas D, Azenha ME, Canle M, Burrows HD (2017) Effect of calcination temperature on the photocatalytic efficiency of acidic sol–gel synthesized TiO_2 nanoparticles in the degradation of alprazolam. Photochem Photobiol Sci 1:1–37
Sabry RS, Al-Haidarie YK, Kudhier MA (2016) Synthesis and photocatalytic activity of TiO_2 nanoparticles prepared by sol–gel method. J Sol Gel Sci Technol 78(2):299–306
Sahel K, Bouhent M, Belkhadem F, Ferchichi M, Dappozze F, Guillard C, Figueras F (2014) Photocatalytic degradation of anionic and cationic dyes over TiO_2 P25, and Ti-pillared clays and Ag-doped Ti-pillared clays. Appl Clay Sci 95:205–210
Sakthivel T, Jagannathan K (2017) Structural, optical, morphological and elemental analysis on sol–gel synthesis of Ni doped TiO_2 nanocrystallites. Mech Mater Sci Eng 9(1):1–5
Sani HA, Ahmad MB, Hussein MZ, Ibrahim NA, Musa A, Saleh TA (2017) Nanocomposite of ZnO with montmorillonite for removal of lead and copper ions from aqueous solutions. Proc Saf Environ Prot 109:97–105
Sdiri AT, Higashi T, Jamoussi F (2014) Adsorption of copper and zinc onto natural clay in single and binary systems. Int J Environ Sci Technol 11:1081–1092
Selman AM, Hassan Z, Husham M (2014) Structural and photoluminescence studies of rutile TiO_2 nanorods prepared by chemical bath deposition method on Si substrates at different pH values. Measurement 56:155–162
Shaban M, Mohamed F, Abdallah S (2018) Production and characterization of superhydrophobic and antibacterial coated fabrics utilizing ZnO nanocatalyst. Sci Rep 8:1–15
Shaikh RS, Rakh RR, Ravangave LS (2016) Sol–gel precipitation synthesis of ZnO nanoparticles, their morphological changes after calcinations and antibacterial properties. Int Res J Sci Eng 4(1):31–35
Sharma A, Karn RK, Pandiyan SK (2014) Synthesis of TiO_2 nanoparticles by sol–gel method and their characterization. J Basic Appl Eng Res 1(9):1–5

Shastri L, Qureshi MS, Malik MM (2014) Synthesis and luminescence properties of ZnO nanoparticles produced by the sol–gel method. J Pure Appl Ind Phys 4(3):119–125

Sheikhnejad-Bishe O, Zhao F, Rajabtabar-Darvishi A, Khodadad E, Mostofizadeh A, Huang Y (2014) Influence of temperature and surfactant on the photocatalytic performance of TiO_2 Nanoparticles. Int J Electrochem Sci 9:4230–4240

Singh PK, Mukherjee S, Ghosh CK, Maitra S (2017) Influence of precursor type on structural, morphological, dielectric and magnetic properties of TiO_2 nanoparticles. Cerâmica 63:549–556

Sips R (1948) On the structure of a catalyst surface. J Chem Phys 16(5):490–495

Sirelkhatim A, Mahmud S, Seeni A, Kaus NHM, Ann LC, Bakhori SKM, Hasan H, Mohamad D (2015) Review on zinc oxide nanoparticles: antibacterial activity and toxicity mechanism. Nano Micro Lett 7:219–242

Smirnova N, Petrik L, Vorobets V, Kolbasov G, Eremenko A (2017) Sol–gel synthesis, photo- and electrocatalytic properties of mesoporous TiO_2 modified with transition metal ions. Nanoscale Res Lett 12:239–247

Soltani RDC, Jorfi S, Ramezani H, Purfadakari S (2016) Ultrasonically induced ZnO–biosilica nanocomposite for degradation of a textile dye in aqueous phase. Ultrasonics Sonochem 28:69–78

Sonawane GH, Patil SP, Shrivastava VS (2016) Photocatalytic degradation of safranine by ZnO–bentonite: photodegradation versus adsorbability. J Inst Eng 98(1):55–63

Sponza DT, Oztekin R (2015) Ciproxin removal from a raw wastewater by nano bentonite-ZnO: comparison of adsorption and photooxidation processes. Recent Adv Environ Biol Eng, pp 18–27

Sun W, Ma G, Sun Y, Liu Y, Song N, Xu Y, Zheng H (2017) Effective treatment of high phosphorus pharmaceutical wastewater by chemical precipitation. Can J Chem Eng 1:1–24

Syngouna VI, Chrysikopoulos CV, Kokkinos P, Tselepi MA, Vantarakis A (2017) Cotransport of human adenoviruses with clay colloids and TiO_2 nanoparticles in saturated porous media: effect of flow velocity. Sci Total Environ 598:160–167

Szczepanik B, Rogala P, Słomkiewicz PM, Banaś D, Kubala-Kukuś A, Stabrawa I (2017) Synthesis, characterization and photocatalytic activity of TiO_2-halloysite and Fe_2O_3-halloysite nanocomposites for photodegradation of chloroanilines in water. Appl Clay Sci 149:118–126

Tan J, Huang Y, Wu Z, Chen X (2017) Ion exchange resin on treatment of copper and nickel wastewater. IOP Conf Ser Earth Environ Sci 94:1–6

Temkin MI, Pyzhev V (1940) Kinetics of ammonia synthesis on promoted iron catalyst. Acta Physicochim 12:327–356

Thangavelu K, Annamalai R, Analnandhi D (2013) Characterization of nanosized TiO powdered by sol-gel precipitation route. Int J Emerg Technol Adv Eng 3(1):636–639

Thirumavalavan M, Huang K, Lee J (2013) Preparation and morphology studies of nano zinc oxide obtained using native and modified chitosans. Materials 6:4198–4212

Tsega M, Dejene FB (2017) Influence of acidic pH on the formulation of TiO_2 nanocrystalline powders with enhanced photoluminescence property. Heliyon 3(2):e00246

Uddin MK (2016) A review on the adsorption of heavy metals by clay minerals, with special focus on the past decade. Chem Eng J 308:438–462

Ullatti SG, Periyat P (2017) Sol–gel synthesis of titanium dioxide. Sol–gel materials for energy. Environ Electron Appl 1:271–283

Unuabonaha EI, Ugwuja CG, Omorogie MO, Adewuyi A, Oladoja NA (2017) Clays for efficient disinfection of bacteria in water. Appl Clay Sci 151:211–223

Vahidhabanu S, Karuppasamy D, Adeogun AI, Babua BR (2017) Impregnation of zinc oxide modified clay over alginate beads: a novel material for the effective removal of Congo red from wastewater. R Soc Chem Adv 7:5669–5678

Vaizoğullar AI (2017) TiO_2/ZnO supported on sepiolite: preparation, structural characterization, and photocatalytic degradation of flumequine antibiotic in aqueous solution. Chem Eng Commun 204(6):689–697

Vanaja A, Rao S (2016) Precursors and medium effect on zinc oxide nanoparticles synthesis by sol–gel process. Int J Appl Nat Sci (IJANS) 5(1):53–62

Venzke CD, Rodrigues MAS, Giacobbo A, Bacher LE, Lemmertz IS, Viegas C, Striving J, Pozzebon S (2017) Application of reverse osmosis to petrochemical industry wastewater treatment aimed at water reuse. Manage Environ Qual Int J 28(1):70–77

Voigt I, Richter H, Weyd M, Milew K, Haseneder R, Günther C, Prehn V (2019) Treatment of oily and salty mining water by ceramic nanofiltration membranes. Chem Ing Tech 91(10):1454–1459

Wang G, Xu D, Guo W, Wei X, Sheng Z, Li Z (2017) Preparation of TiO_2 nanoparticle and photocatalytic properties on the degradation of phenol. In: 2nd international conference on advances in energy resources and environmental engineering. IOP Conference series: Earth Environ Sci, vol 59, pp 1–6

Wang H, Zhou P, Guo R, Wang Y, Zhan H, Yuan Y (2018) Synthesis of rectorite/Fe_3O_4/ZnO composites and their application for the removal of methylene blue dye. Catalyst 8:107–124

Weber WJ, Morris JC (1963) Kinetics of adsorption on carbon from solution. J Sanit Eng Div 89:31–60

WHO (World Health Organization) (2014) Progress on drinking-water and sanitation. WHO, Geneva

World Health Organization (2015) Drinking-water - Fact Sheet No. 391. http://www.who.int/mediacentre/factsheets/fs391/en/. Accessed 4 Feb 2016

Wu A, Wang D, Wei C, Zhang X, Liu Z, Feng P, Ou X, Qiang Y, Garcia H, Niu J (2019) A comparative photocatalytic study of TiO_2 loaded on three natural clays with different morphologies. Appl Clay Sci 183:105352

Xue J, Shen Q, Yang F, Liang W, Liu X (2014) Investigation on the influence of pH on the structure and photoelectrochemical properties of CdSe electrolytically deposited into TiO_2 nanotube arrays. J Alloys Compd 607:163–168

Yahaya MM, Azam MA, Teridi MAM, Singh PK, Mohamad AA (2017) Recent characterization of sol–gel synthesized TiO_2 nanoparticles. INTECH, pp 109–129

Yang C, Zhu Y, Wang J, Li Z, Su X, Niu C (2015) Hydrothermal synthesis of TiO_2-WO_3-bentonite composites: conventional versus ultrasonic pretreatments and their adsorption of methylene blue. Appl Clay Sci 105–106:243–251

Ye J, Li X, Hong J, Chen J, Fan Q (2015) Photocatalytic degradation of phenol over ZnO nanosheets immobilized on montmorillonite. Mater Sci Semicond Proc 39:17–22

Yin Q, Xiang J, Wang X, Guo X, Zhang T (2016) Preparation of highly crystalline mesoporous TiO_2 by sol–gel method combined with two-step calcining process. J Exp Nanosci 11(14):1127–1137

You N, Wang X-F, Li J-Y, Fan H-T, Shen H, Zhang Q (2018) Synergistic removal of arsanilic acid using adsorption and magnetic separation technique based on Fe_3O_4@ graphene nanocomposite. J Ind Eng Chem 70:346–354

You N, Yao H, Wang Y, Fan HT, Wang CS, Sun T (2019) Development and evaluation of diffusive gradients in thin films based on nanosized zinc oxide particles for the in situ sampling of tetracyclines in pig breeding wastewater. Sci Total Environ 651:1653–1660

Yuan GD, Theng BKG, Churchman GJ, Gates WP (2013) Clays and clay minerals for pollution control. In: Bergaya F, Lagaly G (eds) Handbook of clay science, part A, 2nd edn. Elsevier, Amsterdam, pp 587–644

Yudoyono G, Ichzan N, Zharvan V, Daniyati R, Santoso H, Indarto B, Pramono YD, Zainuri M, Darminto (2016) Effect of calcination

temperature on the photocatalytic activity of TiO_2 powders prepared by co-precipitation of $TiCl_3$. In: The 3rd international conference on advanced materials science and technology (ICAMST 2015). AIP conference proceeding, vol 1725, pp 1–7

Yusoff N, Ho L, Ong S, Wong Y, Khalik W, Ridzwan MF (2017) Enhanced photodegradation of phenol by ZnO nanoparticles synthesized through sol–gel method. Sains Malays 46(12):2507–2514

Zahedi Y, Fathi-Achachlouei B, Yousefi AR (2017) Physical and mechanical properties of hybrid montmorillonite/zinc oxide reinforced carboxymethyl cellulose nanocomposites. Int J Biol Macromol 108:863–873 **(in Press)**

Zargar RA, Arora M (2017) Synthesis and characterization of ZnO nanoparticles for biomedical applications. Glob J Nanomed 2(1):1–3

Zekic E, Vukovic Z, Halkijevic I (2018) Application of nanotechnology in wastewater treatment. Građevinar 70(4):315–323

Zen S, El Berrichi FZ (2014) Adsorption of tannery anionic dyes by modified kaolin from aqueous solution. Des Water Treat 57(13):1–9

Zen S, El Berrichi FZ, Abidi N, Duplay J, Jada A, Gasmi B (2018) Activated kaolin's potential adsorbents for the removal of Derma Blue R67 acid dye: kinetic and thermodynamic studies. Desalin Water Treat 112:196–206

Zhang Y, Wu B, Xu H, Liu H, Wang M, He Y, Pan B (2016) Nanomaterials-enabled water and wastewater treatment. NanoImpact 3(4):22–39

Zhu R, Chena Q, Zhou Q, Xi Q, Zhua J, He H (2016) Adsorbents based on montmorillonite for contaminant removal from water: a review. Appl Clay Sci 123:239–258

Zyoud AH, Zorba T, Helal M, Zyoud S, Qamhiya N, Hajamohideen AR, Zyoud S, Hilal HS (2019) Direct sunlight-driven degradation of 2-chlorophenol catalyzed by kaolinite-supported ZnO. Int J Environ Sci Technol 16(10):1–10